Feb 21st 2024

Blocking Interleukin-1β transiently limits left ventricular dilation and reduces cardiac lymphangiogenesis in a mouse pressure-overload model

Heron C.[1], Lemarcis T.[1], Bundalo M.[2,*], Laguerre O.[1,*], Valentin C[1,*], Valet M.[1], Michel JB.[3], Mulder P.[1], Zernecke A.[2,§], Tardif V.[1], Brakenhielm E.[1,§]

[1] Univ Rouen Normandie, INSERM EnVI, UMR1096, F-76000, Rouen, France

[2] Institute of Experimental Biomedicine, University Hospital Würzburg, 97080 Würzburg, Germany.

[3] UMR 1116, Université de Lorraine, INSERM, DCAC, F-54000, Nancy, France

*equal contribution

§corresponding authors

Keywords: Hypertrophy, inflammation, lymphatics, VEGF-C, perivascular fibrosis

Running title: Cardiac and lymphatic impact of anti-IL-1β treatment

Abstract	294 words
Main text, references and legends	7 818 words
Figures & Tables	5 + 2
Suppl. Figs & Tables	5 + 7
References	42

***Corresponding authors**:
Dr. Ebba Brakenhielm, Inserm UMR1096, Normandy University, UniRouen, Faculty of Medicine, 22 Boulevard Gambetta, 76183 Rouen, France

Tel. +33-235-148370; Fax +33-235-148365; email: ebba.brakenhielm@inserm.fr
ORCID: https://orcid.org/0000-0003-3378-8300

Dr. Alma Zernecke, Institute of Experimental Biomedicine, University Hospital Würzburg, 97080 Würzburg, Germany
ORCID: https://orcid.org/0000-0001-8551-4729

The authors declare that no conflict of interest exists

Abstract

Blocking inflammatory pathways, e.g. the inflammasome or interleukin (IL)-1β, is a promising therapeutic approach in heart failure (HF). We hypothesized that IL-1β may stimulate cardiac lymphangiogenesis in response to left ventricular (LV) dilation following pressure-overload. Consequently, blocking IL-1β may reduce lymphangiogenesis, delaying resolution of myocardial edema and inflammation, aggravating cardiac fibrosis, and accelerating HF development.

Here we investigated the effects of anti-IL-1β treatment during HF development following pressure-overload, induced by transaortic constriction (TAC) in BALB/c mice prone to LV dilation. We examined the molecular mechanisms of IL-1β in macrophages and lymphatic endothelial cells, and assessed links between perivascular fibrosis and lymphatics in HF patients with ischemic or dilated cardiomyopathy (DCM).

We found that early anti-IL-1β treatment transiently delayed LV dilation, but did not alter cardiac lymphangiogenesis, hypertrophy, or dysfunction at 8 weeks post-TAC. In contrast, late anti-IL-1β treatment reduced cardiac lymphangiogenesis in response to LV dilation. This was linked to a cell non-autonomous role of IL-1β in promoting cardiac lymphangiogenesis through stimulation of macrophage production and maturation of VEGF-C. Surprisingly, despite reduced lymphatic density in late anti-IL-1β-treated mice, cardiac inflammation, interstitial fibrosis, and dysfunction were not aggravated. Further, we found that perivascular lymphatic density, unaltered by IL-1β, was negatively associated with perivascular fibrosis in HF patients and our TAC model.

In conclusion, IL-1β blockage elicited transient functional cardiac benefit when initiated before onset of LV dilation post-TAC in mice. In contrast, late treatment reduced cardiac lymphangiogenesis, but did not significantly accelerate HF development, likely reflecting lymphatic transport dysfunction post-TAC. Our data suggest that the therapeutic window for anti-IL-1β treatment is crucial, as initiation of treatment during the lymphangiogenic response, induced by LV dilation, may diminish the potential cardiac benefit in HF patients. Finally, our data indicate that IL-1β-independent perivascular lymphangiogenesis may limit perivascular fibrosis.

Introduction

Interleukin-1β (IL-1β) signaling has emerged as a promising therapeutic target to limit inflammation in cardiovascular diseases, as highlighted in the CANTOS study, where *Canakinumab* reduced major adverse cardiovascular events in atherosclerotic patients.[1] Currently, other IL-1β blocking agents, such as *Anakinra*, are being evaluated in the setting of ischemic heart failure (HF)[2]. While IL-1β protein levels also are increased in non-ischemic dilated cardiomyopathy (DCM) HF patients[3], fewer experimental studies have investigated the cardiac impact of IL-1β-targeting in non-ischemic HF, such as following pressure-overload induced by transverse aortic constriction (TAC).

IL-1β not only regulates inflammation and fibrosis (in part by stimulating IL-6), but also impacts cardiac function *directly* due to negative inotropic effects[4]. In addition, IL-1β may stimulate cardiomyocyte hypertrophy *via* upregulation of insulin-like growth factor (*Igf1*)[5]. The potential of IL-1β as a therapeutic target to limit HF development in non-ischemic cardiomyopathy currently remains uncertain. Most recently, CC chemokine receptor-2 (CCR2)-expressing myeloid cells have been suggested as a key source of IL-1β in failing human hearts, and found to be essential for driving cell-fate commitment of cardiac fibroblasts into periostin (Postn)-expressing matrifibroblasts mediating interstitial fibrosis after pressure-overload in mice[6,7]. Promisingly, reduction of cardiac IL-1β production during pressure-overload, by early treatment with a selective pharmacological inflammasome (NLRP3) inhibitor, reduced both cardiac hypertrophy and fibrosis at 5 weeks post-TAC in male C57Bl/6J mice.[8] However, another study, employing an IL-1β-blocking antibody, also post-TAC in male C57Bl/6J mice, demonstrated that the reduction in left ventricular (LV) hypertrophy led to accelerated LV dilation and HF development[9], potentially linked to reduced IL-1β-induced VEGF-A-mediated cardiac angiogenesis in response to cardiac hypertrophy. Similarly, a recent study, based on *Nlrp3* gene deletion in male C57Bl/6J mice, revealed that reduction of early compensatory cardiac hypertrophy following TAC led to accelerated LV dilation and aggravated cardiac dysfunction[10].

Recently, we demonstrated that while pressure-overload leads to compensated concentric hypertrophy in female C57Bl/6J mice, in BALB/c mice, characterized by elevated cardiac *Il1b* gene expression post-TAC, it leads to eccentric hypertrophy with severe LV dilation.[11] Moreover, we demonstrated that LV dilation-induced wall stress,

but not LV hypertrophy *per se*, triggers massive cardiac lymphangiogenesis, which however fails to limit cardiac inflammation and edema.[11] Lymphatics are essential for cardiac function, and consequently cardiac lymphatic dysfunction, or insufficient lymphangiogenesis, has been shown experimentally to contribute to adverse cardiac remodeling, inflammation, and fibrosis following myocardial infarction (MI) or pressure-overload.[12–17] Conversely, inflammatory mediators, including IL-1β, may modulate lymphangiogenesis and/or lymphatic function.[18–20] Interestingly, we previously observed a striking correlation between cardiac *Il1b* and *Vegfc* expression[11], in line with previous reports demonstrating both direct and indirect pro-lymphangiogenic effects of IL-1β in other organs. This includes stimulation of VEGF-C-mediated proliferation of lymphatic endothelial cells (LEC) *via* an autocrine loop[18], as well as IL-1β-mediated activation of VEGF-C-release by macrophages to promote lymphangiogenesis during chronic inflammation in other tissues[21]. In contrast, local inflammation induces lymphatic dysfunction, as pro-inflammatory mediators, including IL-1β, act on lymphatic smooth muscle cells to reduce lymphatic drainage.[22] Additionally, in the heart, where lymphatic drainage depends directly on the force of cardiac contraction[23], the negative inotropic effects of IL-1β may contribute to cardiac lymphatic dysfunction in cardiovascular diseases.

Here, we investigated the impact of anti-IL-1β treatment on cardiac lymphatics and HF development post-TAC in BALB/c mice prone to LV dilation. We hypothesized that elevated cardiac *Il1b* may provide a molecular link between increased wall stress and cardiac lymphangiogenesis in response to pressure-overload. Specifically, we argued that the striking lymphangiogenesis observed in our TAC model may be induced by elevated cardiac IL-1β levels. This would mechanistically couple cardiac wall stress (induced by LV dilation) to local VEGF-C production by cardiac cells, as cardiac fibroblast IL-1β secretion is induced by mechanical stress[5]. We expected that interfering with IL-1β signaling post-TAC may have deleterious effects including *i)* reduction of compensatory cardiac hypertrophy leading to accelerated LV dilation; and *ii)* reduction of cardiac lymphangiogenesis leading to aggravation of inflammation and fibrosis. To investigate the cardiac functional and lymphatic impact of IL-1β in different stages of pressure-overload-induced HF, we applied an anti-IL-1β antibody (*Gevokizumab*) before and after development of LV dilation in BALB/c mice (*early* and *late* treatment, **Fig. 1a**). Further, to dissect the mechanisms involved in IL-1β-induced

lymphangiogenesis, we investigated the molecular effects of cytokine stimulation *in vitro* in macrophage and LEC cultures.

Results

Early, but not late, anti-IL-1β treatment delays LV dilation and dysfunction but does not limit HF development post-TAC.

Evaluation of cardiac function by echocardiography at 3-, 6-, and 8-weeks post-TAC unexpectedly demonstrated that early anti-IL-β treatment transiently prevented LV dilation and dysfunction up to 6 weeks-post-TAC (**Fig. 1b-e**; **Table 1**; **Suppl. Table 1**). Indeed, the reduction in LV hypertrophy index, observed in TAC controls starting from 3 weeks, was delayed in *early*-treated mice (**Fig. 1e**). However, at the end of the study, this beneficial functional cardiac effect was lost, and treated animals displayed similar reduction of fractional shortening (FS) as compared to control TAC mice (**Fig. 1d**). Morphometric and gravimetric measurements at 8 weeks post-TAC revealed no effects of *early*-stage treatment on either TAC-induced cardiac hypertrophy (**Fig. 1f; Suppl. Fig. 1**) or pulmonary edema (**Fig. 1g**).

In contrast, *late* anti-IL-β treatment tended to increase LV dilation (**Fig. 1b, Table 1**), although it did not significantly aggravate cardiac dysfunction, hypertrophy, or pulmonary edema at 8 weeks (**Fig. 1d-g**). Moreover, cardiac gene expression of *Nppa* and *Nppb* (encoding ANP and BNP respectively) were similarly increased, as compared to TAC controls, at 8 weeks post-TAC in both *early* and *late* treated mice (**Fig. 1h**). Evaluation of cardiomyocyte sizes revealed moderate cardiac hypertrophy at 8 weeks post-TAC, which was unaltered by anti-IL-β treatment (**Fig. 1j**).

Only *early* anti-IL-1β treatment moderately affects cardiac inflammation post-TAC

We and others have previously shown biphasic upregulation of cardiac IL-1β during experimental pressure-overload, with a rapid increase (from 3 days post-TAC[21]), followed by a second progressive increase (from 3-8 weeks post-TAC).[11,24] Our cardiac immunohistochemical analyses revealed increased cardiac IL-1β levels, notably in areas of macrophage accumulation and interstitial fibrosis (**Suppl. Fig. 2a**). Pressure-overload not only activates inflammatory pathways in the heart, but also systemic innate immune cell activation, which in the chronic setting leads to splenomegaly. [24,25] We found that both *early* and *late* anti-IL-1β treatment significantly reduced spleen weight at 8 weeks post-TAC (**Fig. 2a**), reflecting systemic anti-inflammatory effects of

the treatment, as we previously described in rats.[26] Only *late* anti-IL-1β treatment led to a compensatory increase in circulating IL-1β plasma levels, as evaluated by ELISA (**Fig. 2b**). Of note, rather than neutralizing the cytokine, *Gevokizumab* acts by reducing IL-1β binding to the IL-1R receptor.[26] In contrast, neither *early* nor *late* treatment altered IL-1β cardiac protein or gene expression levels post-TAC (**Fig. 2c, d**; **Suppl. Fig. 2a**). Unexpectedly, anti-IL-1β treatment did not reduce cardiac gene expression of other proinflammatory cytokines, including *Il6* and *Il33*, evaluated by qPCR, as compared to control TAC mice (**Fig. 2e**). Of note, all three cytokines, and notably *Il6*, correlated with the degree of LV dilation at 8 weeks post-TAC (**Suppl. Fig. 2b-d**).

Concerning the impact of the treatment on cardiac immune cells at 8 weeks post-TAC, neither *early* nor *late* treatment significantly altered total macrophage levels (**Fig. 2f**), as evaluated by immunohistochemistry. However, *early* anti-IL-1β treatment tended to reduce cardiac-infiltrating $CD68^+$ / Lyve-1^- macrophages (**Fig. 2g**). In contrast, neither treatment significantly altered TAC-induced expansion of tissue-resident $CD68^+$/Lyve-1^+ macrophages (**Fig. 2h, i**).

Taken together, the observed limited benefit of *early* anti-IL-1β treatment on cardiac inflammation is in line with the transient and moderate improvement of cardiac dysfunction post-TAC seen in our study. In contrast, our finding that *late* anti-IL-1β treatment did not suffice to reduce cardiac inflammation following pressure-overload indicates that other pro-inflammatory cytokines induced by cardiac wall stretch, such as IL-6[4], may counteract reduced IL-1β signaling, notably in the decompensated phase post-TAC.

Anti-IL-1β treatments alters cardiac lymphangiogenesis post-TAC.

We previously demonstrated that cardiac *Vegfc* gene expression is increased starting from 3-4 weeks post-TAC in BALB/c mice, stimulating cardiac lymphangiogenesis during the subsequent rapid LV dilation occurring in the decompensation phase (6-8 weeks post-TAC).[11] Western blot analysis of cardiac samples at 8 weeks post-TAC revealed that VEGF-C protein levels, specifically the ratio between mature and immature forms of the growth factor, were significantly increased post-TAC as compared to sham mice (**Fig. 3a**), while VEGF-D protein levels were not altered (**Suppl. Fig. 3a**). These results are in line with our previous report that cardiac lymphangiogenesis post-TAC in BALB/c mice is essentially mediated by VEGF-C.[11]

Further, our new data suggest that enhanced maturation of cardiac VEGF-C may occur post-TAC in BALB/c mice. Interestingly, we observed subpopulation-dependent correlation of cardiac macrophage densities and lymphatic densities post-TAC, with infiltrating macrophages potentially exerting deleterious effects, while tissue-resident macrophages were linked to enhanced lymphangiogenesis (**Suppl. Fig. 3b, c**). Similarly, tissue-resident macrophages have recently been proposed as a preferential source of VEGF-C in the heart. [27]

Next, to investigate the impact of IL-1β on macrophage production of VEGF-C, we stimulated bone marrow-derived macrophages with recombinant cytokine for 4h or 24h and analyzed gene expression levels of *Vegfc* and associated genes involved in VEGF-C maturation, such as Adamts3 that cleaves VEGF-C N-terminal propeptide under guidance of Ccbe1[28]. We found that IL-1β induced transient upregulation of *Ccbe1*, while both *Vegfc* and *Adamts3* levels were significantly increased at both 4h and 24h of stimulation (**Table 2**). Further, whereas IL-1β did not impact expression of Cathepsin D (*Ctsd*) or proprotein convertases (*Psck5* or *Psck7*), three additional proteases known to modulate VEGF-C maturation[28], it did stimulate expression of *Furin,* an intracellular proprotein convertase that matures pro-VEGF-C by cleaving its C-terminal propeptide, after 24h of IL-1β stimulation. In agreement, western blot analyses of macrophage-conditioned media revealed an increase in mature VEGF-C levels following IL-1β stimulation (**Suppl. Fig. 4**). In contrast, in murine lymphatic endothelial cells (LECs), which expressed low, but detectable levels of *Il1r1*, IL-1β did not upregulate *Ctsd* or *Furin* (**Suppl. Table 2**). Further, the levels of expression in murine LECs of other proteases involved in VEGF-C maturation were either very low (*Pcsk7*), or undetectable (*Adamts3*, *Adamts14, Pcsk5, Ccebe1*), both at baseline and after IL-1β. In addition, whereas *Vegfc* was not readily quantifiable in LECs, *Vegfd* expression was not influenced by IL-1β. In contrast, *Flt4* levels were increased (**Suppl. Table 2**). These findings thus support a majoritarian cell non-autonomous role of IL-1β in stimulation of lymphangiogenesis in the heart. Further, our data are in line with previous reports demonstrating a key role of macrophages in regulation of cardiac lymphangiogenesis post-TAC[27] as well as after MI[29].

As mentioned above*, early* anti-IL-1β treatment reduced infiltrating macrophage levels post-TAC, and we found that this potentiated lymphatic capillary expansion at 8 weeks (**Fig. 3b, Suppl. Fig. 5**). However, the treatment did not modify cardiac VEGF-C levels

(**Fig. 3a**), open vessel densities, or sizes at 8 weeks (**Fig. 3c, d**). Moreover, cardiac gene expression analysis revealed that *early* anti-IL-1β treatment did not alter levels of key lymphatic markers and regulators (*Pdpn*, *Ccl21*, *Lyve1*, *Vegfc*, and *Vegfd*) as compared to control TAC mice (**Suppl. Table 3**).

In contrast, in agreement with our *in vitro* data in macrophages supporting our hypothesis of a role of IL-1β in linking LV dilation to stimulation of lymphangiogenesis, we found that *late* anti-IL-1β, initiated at 4 weeks post-TAC, before LV dilation, potently reduced cardiac levels of mature VEGF-C (**Fig. 3a**), leading to reduced lymphangiogenesis at 8 weeks (**Fig. 3b, c, Suppl. Fig. 5**) despite pronounced LV dilation in both *late*-treated and TAC control groups (**Fig. 1b, c**). Interestingly, while lymphatic capillary and precollector (open vessel) densities were reduced, lymphatic vessel sizes were increased (**Fig. 3d**). This enlargement of lymphatics ("profile switch" from 5-20 µm size range to 20-50 µm vessel diameters (**Suppl. Fig. 3d**)) was sufficient to partially compensate for the reduction in lymphangiogenesis following anti-IL-1β treatment, and total cardiac lymphatic areas remained unchanged, as compared to TAC controls (**Fig. 3e**). In contrast, coronary perivascular lymphatic density, increased post-TAC, was not altered by either *early* or *late* anti-IL-1β treatment (**Fig. 3f**).

Although cardiac expression analyses indicated that *late* anti-IL-1β treatment reduced *Vegfd* levels (**Suppl. Table 3**), western blot analyses of VEGF-D did not confirm this (**Suppl. Fig. 3a**). Further, despite the reduced lymphatic density, we found that *late* anti-IL-1β treatment increased cardiac *Lyve1* and *Ccl21* gene expression, as compared to control TAC mice (**Suppl. Table 2**). However, immunohistochemical analyses revealed that CCL21 lymphatic gradients were not increased, but paradoxically decreased in *late*-treated mice (**Fig. 3g, h**). Notably, reduced CCL21 gradients may limit lymphatic drainage of $CCR7^+$ immune cells, including macrophages. However, as noted previously, we did not observe any increase in cardiac macrophage levels at 8 weeks in *late* anti-IL-1β-treated mice as compared to TAC controls. Thus, the mechanisms, and functional relevance, of reduced cardiac lymphatic CCL21 gradients in *late* anti-IL-1β-treated mice remain to be investigated. Moreover, given these discrepancies noted between cardiac gene and protein expression levels in *late* anti-IL-1β-treated mice, it is possible that inhibition of IL-1β may have influenced cardiac proteases also related to CCL21 maturation[30].

Early, but not late, anti-IL-1β treatment modulates cardiac fibrosis post-TAC

Cardiac inflammation and edema, if unresolved by lymphatic drainage from the cardiac interstitium, may aggravate cardiac fibrosis.[23] Our recent study highlighted that while interstitial fibrosis occurred at 8 weeks post-TAC in BALB/c mice, they were protected against perivascular fibrosis, as compared with C57Bl/6J mice.[11] We proposed that this may be due to expansion of perivascular lymphatics noted only in the former. In support, we found negative correlation (*p=0.04*) between the extent of coronary perivascular fibrosis and perivascular lymphatic densities (**Fig. 4a**). This suggests that IL-1β-independent perivascular lymphangiogenesis during pressure-overload may prevent perivascular fibrosis locally, despite generalized lymphatic dysfunction in the heart contributing to unresolved inflammation and edema driving interstitial fibrosis post-TAC. We previously reported increased lymphatic density around coronaries in clinical biopsies from HF patients, especially in the setting of DCM.[11] Histological analyses revealed that this was associated with lower levels of perivascular fibrosis in DCM as compared to ischemic HF patients (**Fig. 4b, c**), as evaluated in small arterioles (**Fig. 4d, e**). Interestingly, while our study is the first to show a negative correlation between lymphatics and fibrosis in the perivascular niche, previous studies have also reported low levels of perivascular fibrosis in DCM patients.[31]

In our experimental study, we found that while *early* anti-IL-1β treatment slightly reduced cardiac-infiltrating macrophages, it unexpectedly increased interstitial fibrosis as compared to control TAC mice (**Fig 4f**). This would suggest potential beneficial immune effects of IL-1β in the semi-acute phase (1-5 weeks) post-TAC, contributing to the delay in TAC-induced LV dilation. However, this transient prevention of LV dilation led to accelerated changes in LV wall remodeling between 6-8 weeks post-TAC. Thus, chronic phase hyper-activation of mechanical-stress responses in LV matrifibroblasts may have contributed to aggravate interstitial fibrosis at 8 weeks in *early* anti-IL-1β treated mice. In contrast, neither *early* nor *late* anti-IL-1β treatments altered TAC-induced development of replacement fibrosis (micro-scars) (**Fig. 4g**) or perivascular fibrosis (**Fig. 4h**), as evaluated in 16-60 µm in diameter coronary segments (**Fig. 4i**).

Discussion

In this study, we demonstrated that anti-IL-1β treatment with *Gevokuzimab* during pressure-overload did not significantly alter chronic cardiac inflammation, nor was it sufficient to durably prevent deleterious cardiac remodeling, fibrosis, or HF development post-TAC in BALB/c mice. In contrast, in line with our hypothesis, we found that IL-1β appears to play a key role in the cardiac lymphangiogenic response induced by LV dilation. This lymphatic expansion is triggered in the chronic stage following pressure-overload, between 4-8 weeks post-TAC in BALB/c mice. Our data revealed that *late* anti-IL-1β treatment reduced TAC-induced cardiac lymphangiogenesis, without altering cardiac macrophage levels or *Vegfc* gene expression in the heart. Instead, our data showed reduced cardiac mature VEGF-C protein levels in *late*-treated TAC mice. Our *in vitro* macrophage study supports a direct role of IL-1β in promoting both *Vegf-c* expression and VEGF-C maturation, linked to upregulation of *Furin*, *Ccbe1*, and *Adamts3*. In contrast, *early* anti-IL-1β treatment, discontinued week-5 post-TAC, did not reduce cardiac lymphangiogenesis. Indeed, surprisingly, it slightly increased lymphatic capillary, but not precollector, densities. Potentially, this reflects a deleterious impact of infiltrating macrophages, reduced by *early* anti-IL-1β treatment, on cardiac lymphangiogenesis during chronic pressure-overload. Alternatively, as LV dilation was transiently delayed up to 6 weeks post-TAC, it is possible that the subsequent accelerated increase in cardiac wall stress upon termination of treatment may have led to increased *Vegfc* expression in *early* treated mice. However, at 8 weeks, we did not find any differences in cardiac lymphangiogenic growth factor gene or protein levels in *early*-treated mice versus TAC controls. Another potential mechanism is that cardiac IL-1β may exert deleterious effects on lymphatic function post-TAC before the onset of lymphangiogenesis. *Early* anti-IL-1β treatment could then modify lymphatic capillary reactivity to lymphangiogenic factors, despite similar lymphangiogenic stimuli in the decompensating phase post-TAC. Further studies are needed to investigate this possibility.

The pro-lymphangiogenic effects of IL-1β appear to be mainly *indirect*, similar as previously described in mice with tracheal *Il1b*-overexpression.[21] In this setting, blockage of VEGF-C/-D signaling, with soluble VEGFR-3, sufficed to inhibit the pro-lymphangiogenic effects of IL-1β, demonstrating its dependency on the VEGFR-3 axis. The authors further demonstrated that IL-1β stimulated tissue-recruitment of

macrophages, and increased their release of VEGF-C. In contrast, we found a negative correlation between infiltrating cardiac macrophages and lymphatic densities post-TAC. Thus, in our study, cardiac IL-1β did not stimulate lymphangiogenesis post-TAC by promoting cardiac recruitment of macrophages. Instead, in line with a previous report in C57Bl/6 mice[27], we found weak, but positive, correlation between densities of tissue-resident cardiac macrophages and lymphatics. However, IL-1β does not appear as a major regulator of LYVE1^{+} tissue-resident cardiac macrophage expansion, as neither *early* nor *late* phase blockage of IL-1β post-TAC altered densities of this subpopulation. Instead, our *in vitro* data indicated that IL-1β may influence macrophage activity rather than numbers, by promoting VEGF-C maturation. We demonstrate that IL-1β stimulation of macrophages, but not LECs, led to upregulation of proteases, including *Furin* and *Adamts3*, which play key roles in VEGF-C maturation. Of note, recent cardiac single cell RNA sequencing (scRNAseq) analyses suggest that IL-1β may also regulate extracellular matrix remodeling by increasing cardiac fibroblast expression of endogenous protease inhibitors, such as TIMPs[6,7]. Conversely, inhibition of IL-1β signaling in the clinic has been found to reduce tissue plasminogen activator plasma levels.[32] Another potential mechanism of IL-1β is *direct* activation of LECs *via* IL-1R. This would enhance LEC NFκB signaling, promoting increased *Flt4* expression thus sensitizing LECs to VEGF-C produced in autocrine or paracrine manners[33]. However, our unpublished molecular analyses revealed that only 1-2% of cardiac LECs express IL-1R1, and this was not significantly altered after TAC. Our *in vitro* studies in murine LECs confirm low *Il1r1* expression, which nevertheless was sufficient for IL-1β to upregulate *Flt4* expression (1.5 fold-change) in LECs.

In addition to stimulating macrophage-dependent VEGF-C-mediated lymph-angiogenesis post-TAC, our *ex vivo* data indicate that IL-1β may influence lymphatic immune cell recruitment by stimulating CCL21 release in LECs. Interestingly, while cardiac *Ccl21* gene expression increased in *late* anti-IL-1β treated mice, we showed that lymphatic CCL21 chemokine gradients were reduced. This is expected to limit immune cell drainage from the heart, slowing inflammatory resolution. Indeed, CCL21 is the main chemokine released by LECs, and its receptor, CCR7, is expressed in both lymphoid and myeloid cells [34-35]. Our *in silico* analysis of recently published scRNAseq data on cardiac-infiltrating immune cells from C57Bl/6J mice post-TAC[36] or post-MI[37] indicate that in the heart, both B and T cells have elevated *Ccr7* expression. We

previously showed, by flow cytometry in BALB/c mice at 8 weeks post-TAC, that cardiac B cell levels are low, but there is retention post-TAC of macrophages and T cells, especially $CD4^+$ T cells.[11] Thus, reduced lymphatic CCL21 levels, together with reduced lymphatic density following inhibition of IL-1β, could potentially increase cardiac T cell retention post-TAC. Intriguingly, our preliminary data indicate a decrease, rather than an increase, in cardiac T cells in anti-IL-1β-treated TAC mice. This may reflect reduction of local inflammatory processes in the heart by anti-IL-1β treatment, leading to reduced T cell recruitment or expansion. We also expected that the treatment would limit cardiac pro-inflammatory macrophage infiltration post-TAC, and potentially increase tissue-resident macrophage proliferation, known to be cardioprotective post-TAC.[27] However, we found no differences in cardiac-resident $CD68^+$/Lyve-1^+ macrophage levels in either *early* or *late*-treated groups. Further, only *early* anti-IL-1β treatment was associated with a slight decrease in cardiac-infiltrating $CD68^+$/Lyve-1^- macrophage levels. Importantly, in *late*-treated mice, where IL-1β-mediated-lymphangiogenesis was inhibited, the absence of significant effects on cardiac macrophage levels suggests generalized dysfunction of cardiac lymphatics post-TAC. Indeed, we previously showed that the extensive cardiac lymphatic network post-TAC in BALB/c mice is inefficient to resolve cardiac edema, inflammation, or interstitial fibrosis, and thus fails to prevent LV dilation and HF development.[11] Our current study further indirectly demonstrates that cardiac lymphatic function post-TAC is not improved by *late* anti-IL-1β treatment.

We were surprised by the absence of functional cardiac effects of anti-IL-1β treatment at 8 weeks post-TAC, although *early* anti-IL-1β treatment transiently delayed LV dilation, with beneficial functional effects persisting up to 6 weeks post-TAC. These results contrast with previous studies demonstrating that *Nlrp3* gene deletion, which reduced IL-1β production, or early anti-IL-1β antibody therapy, accelerated cardiac dysfunction post-TAC in C57Bl/6J mice, despite reducing cardiac hypertrophy, macrophage infiltration, and fibrosis.[9,10] It appears that prevention of adaptive hypertrophy, mediated by low levels of IL-1β in C57Bl/6J mice, may promote subsequent development of LV dilation and dysfunction post-TAC, potentially due to increased wall stress. Additionally, the authors suggested insufficient angiogenesis matching cardiac hypertrophy as a driver of accelerated cardiac dysfunction in *Nlrp3*-deficient or anti-IL-1β treated mice[9,10]. In contrast, in BALB/c mice, pressure-overload

does not lead to extensive hypertrophy, thus lessening the role of cardiac angiogenesis and the functional impact of potential anti-hypertrophic effects of anti-IL-1β treatment. Indeed, our previous studies have revealed maintenance, but not expansion, of blood vascular networks post-TAC in BALB/c mice.[11] *Of note, Gevokizumab* decreases the binding affinity of IL-1β to IL-1R, resulting in a 30-fold reduction of IL-1β signaling, but it does not completely block IL-1β signaling, different from *Canakinumab* and *Anakinra*.[38] We expect that in our study *early* anti-IL-1β treatment may have reduced, but not completely blocked, cardiac IL-1β signaling, thus maintaining weak but beneficial compensatory hypertrophy[5], while transiently blocking the detrimental direct cardiac effects caused by elevated levels of IL-1β. It is possible that *early* and *prolonged* anti-IL-1β treatment would have been required in our study to reach durable benefit on cardiac function. However, long-term treatment, including during LV dilation, would have reduced cardiac lymphangiogenesis, thus potentially confounding beneficial cardiac effects of IL-1β blockage. Of note, the risk for an immune response directed against a therapeutic antibody prevents long-term treatment with *Gevokizumab* in mice.

Other cytokines, including IL-6, may be involved in the pathophysiology of the DCM-like phenotype post-TAC in BALB/c mice. IL-6 has been shown to drive both cardiac fibrosis and pathological hypertrophy following pressure-overload in C57Bl/6 mice.[39] We found that anti-IL-1β treatment did not reduce cardiac *Il6* expression, which may have contributed to the lack of beneficial effects on cardiac fibrosis and HF development found in both *early*- and *late*-treated mice. Importantly, the lack of cardiac benefit of *late* anti-IL-1β treatment in our study suggests that in patients with chronic pressure-overload IL-1β-blocking therapy may be inefficient, and potentially deleterious, by reducing cardiac lymphatic density, if initiated during the process of LV dilation. Intriguingly, the beneficial perivascular lymphangiogenesis occurring post-TAC, which seems to protect against perivascular fibrosis, was not influenced by anti-IL-1β treatment. In agreement, recent scRNAseq analyses coupled to spatial transcriptomics revealed that perivascular fibroblasts, different from Postn^{+} matrifibroblasts, have little interaction with cardiac-infiltrating IL-1β-producing CCR2^{+} myeloid cells[6]. Further studies are thus needed to identify the triggers of perivascular lymphangiogenesis in the heart and to unravel how these lymphatics act to potentially prevent perivascular fibrosis during HF development. Notably, a histological marker of

edema would be required to investigate if these expanded lymphatics surrounding coronary arterioles suffice to locally restore perivascular pressure-gradients caused by excessive blood vascular leakage, which occurs during pressure-overload[11].

Taken together, our study provides, for the first time, a molecular mechanism linking LV dilation to lymphatic remodeling following pressure-overload (**Fig. 5**). Moreover, our data suggest that IL-1β may influence not only lymphatic expansion, but also lymphatic expression profiles or secretomes. Intriguingly, the absence of deleterious cardiac effects following inhibition of lymphangiogenesis by *late* anti-IL-1β treatment is in support of our previous finding that the expanded lymphatic network in BALB/c mice post-TAC appears dysfunctional and/or immature[11]. In contrast, we and other have demonstrated that inhibition of lymphangiogenesis during pressure-overload in C57Bl/6J mice and in Wistar rats, by *Flt4* deletion or anti-VEGFR-3 treatment, aggravates cardiac inflammation and dysfunction.[11,17,40,41] Further investigations are needed to determine why IL-1β-mediated lymphangiogenesis leads to aberrant hyper-sprouting and dysfunctional cardiac lymphatics in BALB/c mice. Molecular analyses are underway to determine how expanded cardiac lymphatics post-TAC differ from healthy lymphatics in BALB/c mice, in order to identify new targets to treat lymphatic dysfunction in HF.

As for the clinical outlook, a recent case-report in a stage III HF patient, secondary to idiopathic inflammatory DCM, demonstrated rapid improvement of LV function following *Anakinra* treatment, associated with reduced IL-6 and BNP levels.[42] We speculate that this cardiac benefit of IL-1β inhibition in an already severely dilated heart may also be related to reduction of negative inotropic effects of the cytokine. In our study, we cannot exclude that the observed inhibition of lymphangiogenesis may have contribute to the lack of functional cardiac benefit of anti-IL-1β in *late*-treated mice. Thus, anti-IL-1β may have a dual therapeutic window where targeting of IL-1β in the early stage, before LV dilation, or alternatively at later stages of the disease, when LV dilation and cardiac lymphangiogenesis are well-established, may be required to obtain clinical benefit in HF patients.

Material and Methods

Study approval

Animal experiments performed in this study were approved by the regional Normandy ethics review board in line with E.U and French legislation (APAFIS #23175-2019112214599474 v6, #32433-2022070715208369 v2). A total of 88 BALB/c female mice, surviving TAC or sham-surgery were included in this study. Anonymized human heart samples evaluated in this study were collected with informed consent by the Bichat hospital biobank (*U1148 BB-0033-00029/* BBMRI, coordinator JB Michel) authorized for tissue collection by the Inserm institutional review board as previously reported[11].

Experimental mouse model, macrophage cell culture, and human samples

TAC surgery was performed in adult female BALB/c mice (Janvier Laboratories, France). Briefly, a minimally invasive method was used to constrict the aortic arch, using a 26G needle. Double-banding of the aorta was applied to prevent suture internalization and model variability, as described.[11] Anti-IL-1β treatment consisted of repeated intraperitoneal injections of a blocking monoclonal antibody against IL-1β, (Gevokizumab/XOMA-052 provided by Servier France), as previously described[26], using a dose of 200 µg/mouse (10 mg/kg^{-1}) three times per week starting from week-1 until week-5 post-TAC (*early* treatment) or starting from week-4 until week-8 post-TAC (*late* treatment).

Bone marrow-derived macrophages (BMM) were prepared from C57/BL6 mice and cultured, as described[37]. Briefly, serum-starved BMMs were seeded in 6-well plates (6×10^6/well) and exposed to 10 ng/mL recombinant mouse IL-1β (PreproTech). After 4h or 24h of culture, cells were recovered and RNA extracted for qPCR analyses. Balb/c dermal LECs (CellBiologics, BALB-5064L) were seeded in 6-well plates (3×10^5/well) and grown to confluence, serum-starved overnight, and exposed to 20 ng/mL recombinant mouse IL-1β (PreproTech). After 24h cells were recovered and RNA extracted for RNAseq analyses (Novogene). For details see *Suppl. Methods*.

Cardiac samples from end-stage HF patients (recipients of cardiac transplants at the Bichat Hospital in Paris, France) were examined by histology (Sirius Red staining). Discarded cardiac autopsy samples, obtained from age-matched donors without cardiovascular disease, were used as healthy controls, as previously reported[11].

Cardiac functional, cellular, and molecular analyses

Cardiac function was evaluated by echocardiography as described.[11] Cardiac sections were analyzed by histology and immunohistochemistry, as described,[11] to determine lymphatic vessel densities and sizes, immune cell infiltration (macrophages), cardiomyocyte hypertrophy, and fibrosis (Sirius Red staining). Perivascular fibrosis was defined as the area of perivascular fibrosis surrounding the media in similar-sized arterioles, as described.[31] Cardiac gene expression was analyzed by RT-qPCR, and Protein levels of VEGF-C and VEGF-D were assessed by Western Blot. Cardiac and plasma levels of IL-1β were evaluated by ELISA (RnD Systems: ELISA DuoSet anti-IL-1β /IL-1F2 #DY401-05). For details see *Suppl. Methods*.

Statistics

Data are presented as mean ± s.e.m. Comparisons were selected to determine: 1) impact of pathology (healthy sham *vs*. TAC); 2) effect of treatment (anti-IL-1β-treated vs. TAC controls): 3) effect of IL-1β treatment vs. control untreated macrophages. Statistical analyses for comparisons of two independent groups were performed using either Student's two-tailed t-test for groups with normal distribution, or alternatively by Mann Whitney U test for samples where normality could not be ascertained based on D'Agostino & Pearson omnibus normality test. For comparisons of three groups or more either one-way ANOVA followed by Sidak's multiple comparison posthoc (for parameters with n>7 with normal distribution), or alternatively Kruskal-Wallis nonparametric analysis followed by Dunn's posthoc for multiple comparison (for parameters with non-Gaussian distribution) were performed. Longitudinal echocardiography studies were analyzed by paired two-way ANOVA followed by Dunnett's posthoc, while morphometric data and gene expression data were analyzed by two-way ANOVA followed by Sidak's posthoc for multiple pair-wise comparisons or Dunnett's posthoc to compare 3 or more groups. Non-parametric Spearman rank order tests were used for evaluating correlations. Outlier samples were identified as an individual value exceeding group mean±4SD in groups with n≥7. All analyses were performed using GraphPad Prism software.

Author contributions

C.H, O.L, and T.L performed and analyzed immunohistochemistry and histology. Echocardiography was performed and analyzed by C.H and T.L; microgravimetry was

carried out by C.H and T.L; M.B and A.Z designed and carried out *in vitro* macrophage assays and expression analyses; M.V carried out surgical mouse model; C.H carried-out cardiac gene expression analyses; O.L and C.V carried out *in vitro* LEC assays and expression analyses; C.H and C.V performed protein analysis by ELISA and Western Blot; JB.M managed the biobank at Bichat Hospital and contributed clinical data for this study; P.M, A.Z, and V.T participated in study design; A.Z contributed critical comments on the manuscript draft; C.H. and E.B designed the study, analyzed results, and prepared the manuscript draft. All authors approved of the final version of the manuscript.

Acknowledgments

We thank Arantxa González Miqueo, (FIMA, Pamplona, Spain) for helpful discussion on fibrosis; and Anais Dumesnil, Saida Morchid Azhar, Nousayba Ouattara, and Héloïse Quesnel (Normandy University, Rouen, France) for technical assistance with histological analysis, Western blot, and RTqPCR.

Funding

C.H, T.L, and C.V were funded by fellowships from the Normandie Doctoral School (EdNBISE). This work was supported by the Fondation pour la Recherche Médicale (FRM) [*FDT202204014960*] to C.H. V.T was funded by the Chair of Excellence program "*Lymphcosign*" from the Normandy Region (RIN Recherche). The research leading to these results benefitted from funding (E.B) from the ERA-CVD Research Programme, which is a transnational R&D programme jointly funded by national funding organisations [*ANR-16-ECVD-0004*] within the framework of the ERA-NET ERA-CVD. This work is part of the FHU-CARNAVAL supported by a grant from the GCS G4 and labeled by AVIESAN. This work was further supported by a joint grant (E.B, A.Z) from the Agence Nationale de la Recherche (ANR) with the Deutsche ForschungsGemeinschaft (DFG) for the project "CITE-LYMPH" [*ANR-22-CE92-0040-001*; DFG project number 505700170], and DFG projects 453989101 – SFB1525 and 324392634 - TRR221 (A.Z.). The project also benefitted from generalized institutional funds (Inserm U1096 laboratory) from French Inserm and the Normandy Region (CPER 2021, 2022) together with the EU-Normandy region co-funding (2019 7D MICROSCOPY) "*L'Europe s'engage en Normandie avec le Fonds Européen de Développement Régional*".

Conflict of Interest

The authors declare that they have no conflict of interest.

References

1. Ridker, P. M. *et al.* Antiinflammatory Therapy with Canakinumab for Atherosclerotic Disease. *N Engl J Med* **377**, 1119–1131 (2017).
2. Abbate, A. *et al.* Interleukin-1 and the Inflammasome as Therapeutic Targets in Cardiovascular Disease. *Circ Res* **126**, 1260–1280 (2020).
3. Zeng, C. *et al.* NLRP3 inflammasome-mediated pyroptosis contributes to the pathogenesis of non-ischemic dilated cardiomyopathy. *Redox Biol* **34**, 101523 (2020).
4. Li, H., Chen, C. & Wang, D. W. Inflammatory Cytokines, Immune Cells, and Organ Interactions in Heart Failure. *Front Physiol* **12**, 695047 (2021).
5. Honsho, S. *et al.* Pressure-mediated hypertrophy and mechanical stretch induces IL-1 release and subsequent IGF-1 generation to maintain compensative hypertrophy by affecting Akt and JNK pathways. *Circ Res* **105**, 1149–1158 (2009).
6. Amrute, J. M. *et al. Targeting the Immune-Fibrosis Axis in Myocardial Infarction and Heart Failure*. http://biorxiv.org/lookup/doi/10.1101/2022.10.17.512579 (2022) doi:10.1101/2022.10.17.512579.
7. Alexanian, M. *et al. Chromatin Remodeling Drives Immune-Fibroblast Crosstalk in Heart Failure Pathogenesis*. http://biorxiv.org/lookup/doi/10.1101/2023.01.06.522937 (2023) doi:10.1101/2023.01.06.522937.
8. Sano, S. *et al.* Tet2-Mediated Clonal Hematopoiesis Accelerates Heart Failure Through a Mechanism Involving the IL-1β/NLRP3 Inflammasome. *J Am Coll Cardiol* **71**, 875–886 (2018).
9. Higashikuni, Y. *et al.* Toll-like receptor-2 mediates adaptive cardiac hypertrophy in response to pressure overload through interleukin-1β upregulation via nuclear factor κB activation. *J Am Heart Assoc* **2**, e000267 (2013).
10. Higashikuni, Y. *et al.* NLRP3 Inflammasome Activation Through Heart-Brain Interaction Initiates Cardiac Inflammation and Hypertrophy During Pressure Overload. *Circulation* **147**, 338–355 (2023).
11. Heron, C. *et al.* Regulation and impact of cardiac lymphangiogenesis in pressure-overload-induced heart failure. *Cardiovasc Res* **119**, 492–505 (2023).
12. Henri, O. *et al.* Selective Stimulation of Cardiac Lymphangiogenesis Reduces Myocardial Edema and Fibrosis Leading to Improved Cardiac Function Following Myocardial Infarction. *Circulation* **133**, 1484–1497; discussion 1497 (2016).
13. Vieira, J. M. *et al.* The cardiac lymphatic system stimulates resolution of inflammation following myocardial infarction. *J Clin Invest* **128**, 3402–3412 (2018).
14. Houssari, M. *et al.* Lymphatic and Immune Cell Cross-Talk Regulates Cardiac Recovery After Experimental Myocardial Infarction. *Arterioscler Thromb Vasc Biol* **40**, 1722–1737 (2020).
15. Trincot, C. E. *et al.* Adrenomedullin Induces Cardiac Lymphangiogenesis After Myocardial Infarction and Regulates Cardiac Edema Via Connexin 43. *Circ Res* **124**, 101–113 (2019).
16. Song, L. *et al.* Lymphangiogenic therapy prevents cardiac dysfunction by ameliorating inflammation and hypertension. *Elife* **9**, e58376 (2020).

17. Yang, G.-H. *et al.* Overexpression of VEGF-C attenuates chronic high salt intake-induced left ventricular maladaptive remodeling in spontaneously hypertensive rats. *Am J Physiol Heart Circ Physiol* **306**, H598-609 (2014).
18. Weichand, B. *et al.* S1PR1 on tumor-associated macrophages promotes lymphangiogenesis and metastasis via NLRP3/IL-1β. *J Exp Med* **214**, 2695–2713 (2017).
19. Watari, K. *et al.* Role of macrophages in inflammatory lymphangiogenesis: Enhanced production of vascular endothelial growth factor C and D through NF-kappaB activation. *Biochem Biophys Res Commun* **377**, 826–831 (2008).
20. Sáinz-Jaspeado, M. & Claesson-Welsh, L. Cytokines regulating lymphangiogenesis. *Curr Opin Immunol* **53**, 58–63 (2018).
21. Baluk, P. *et al.* Transgenic overexpression of interleukin-1β induces persistent lymphangiogenesis but not angiogenesis in mouse airways. *Am J Pathol* **182**, 1434–1447 (2013).
22. Scallan, J. P., Zawieja, S. D., Castorena-Gonzalez, J. A. & Davis, M. J. Lymphatic pumping: mechanics, mechanisms and malfunction. *J Physiol* **594**, 5749–5768 (2016).
23. Brakenhielm, E., González, A. & Díez, J. Role of Cardiac Lymphatics in Myocardial Edema and Fibrosis: JACC Review Topic of the Week. *J Am Coll Cardiol* **76**, 735–744 (2020).
24. Kleiner, J. L. *et al.* Characterization of Transverse Aortic Constriction in Mice Based on the Specific Recruitment of Leukocytes to the Hypertrophic Myocardium and the Aorta Ascendens. *Mediators Inflamm* **2021**, 1376859 (2021).
25. Patel, B., Ismahil, M. A., Hamid, T., Bansal, S. S. & Prabhu, S. D. Mononuclear Phagocytes Are Dispensable for Cardiac Remodeling in Established Pressure-Overload Heart Failure. *PLoS One* **12**, e0170781 (2017).
26. Harouki, N. *et al.* The IL-1β Antibody Gevokizumab Limits Cardiac Remodeling and Coronary Dysfunction in Rats With Heart Failure. *JACC Basic Transl Sci* **2**, 418–430 (2017).
27. Bizou, M. *et al.* Cardiac macrophage subsets differentially regulate lymphatic network remodeling during pressure overload. *Sci Rep* **11**, 16801 (2021).
28. Künnapuu, J., Bokharaie, H. & Jeltsch, M. Proteolytic Cleavages in the VEGF Family: Generating Diversity among Angiogenic VEGFs, Essential for the Activation of Lymphangiogenic VEGFs. *Biology (Basel)* **10**, 167 (2021).
29. Glinton, K. E. *et al.* Macrophage-produced VEGFC is induced by efferocytosis to ameliorate cardiac injury and inflammation. *J Clin Invest* **132**, e140685 (2022).
30. Loef, E. J., Sheppard, H. M., Birch, N. P. & Dunbar, P. R. Plasminogen and plasmin can bind to human T cells and generate truncated CCL21 that increases dendritic cell chemotactic responses. *J Biol Chem* **298**, 102112 (2022).
31. Dai, Z., Aoki, T., Fukumoto, Y. & Shimokawa, H. Coronary perivascular fibrosis is associated with impairment of coronary blood flow in patients with non-ischemic heart failure. *J Cardiol* **60**, 416–421 (2012).
32. Boermeester, M. A. *et al.* Interleukin-1 blockade attenuates mediator release and dysregulation of the hemostatic mechanism during human sepsis. *Arch Surg* **130**, 739–748 (1995).
33. Zhu, G. *et al.* Lipopolysaccharide increases the release of VEGF-C that enhances cell motility and promotes lymphangiogenesis and lymphatic metastasis through the TLR4-NF-κB/JNK pathways in colorectal cancer. *Oncotarget* **7**, 73711–73724 (2016).

34. Tal, O. *et al.* DC mobilization from the skin requires docking to immobilized CCL21 on lymphatic endothelium and intralymphatic crawling. *J Exp Med* **208**, 2141–2153 (2011).
35. Bromley, S. K., Thomas, S. Y. & Luster, A. D. Chemokine receptor CCR7 guides T cell exit from peripheral tissues and entry into afferent lymphatics. *Nat Immunol* **6**, 895–901 (2005).
36. Martini, E. *et al.* Single-Cell Sequencing of Mouse Heart Immune Infiltrate in Pressure Overload-Driven Heart Failure Reveals Extent of Immune Activation. *Circulation* **140**, 2089–2107 (2019).
37. Rizzo, G. *et al.* Dynamics of monocyte-derived macrophage diversity in experimental myocardial infarction. *Cardiovasc Res* **119**, 772–785 (2023).
38. Issafras, H., Corbin, J. A., Goldfine, I. D. & Roell, M. K. Detailed mechanistic analysis of gevokizumab, an allosteric anti-IL-1β antibody with differential receptor-modulating properties. *J Pharmacol Exp Ther* **348**, 202–215 (2014).
39. Lai, N. C. *et al.* Pressure overload-induced cardiac remodeling and dysfunction in the absence of interleukin 6 in mice. *Lab Invest* **92**, 1518–1526 (2012).
40. Lin, Q.-Y., Zhang, Y.-L., Bai, J., Liu, J.-Q. & Li, H.-H. VEGF-C/VEGFR-3 axis protects against pressure-overload induced cardiac dysfunction through regulation of lymphangiogenesis. *Clin Transl Med* **11**, e374 (2021).
41. Bai, J. *et al.* Angiotensin II Induces Cardiac Edema and Hypertrophic Remodeling through Lymphatic-Dependent Mechanisms. *Oxid Med Cell Longev* **2022**, 5044046 (2022).
42. De Luca, G., Campochiaro, C., Dinarello, C. A., Dagna, L. & Cavalli, G. Treatment of Dilated Cardiomyopathy With Interleukin-1 Inhibition. *Ann Intern Med* **169**, 819–820 (2018).

Figures & Legends

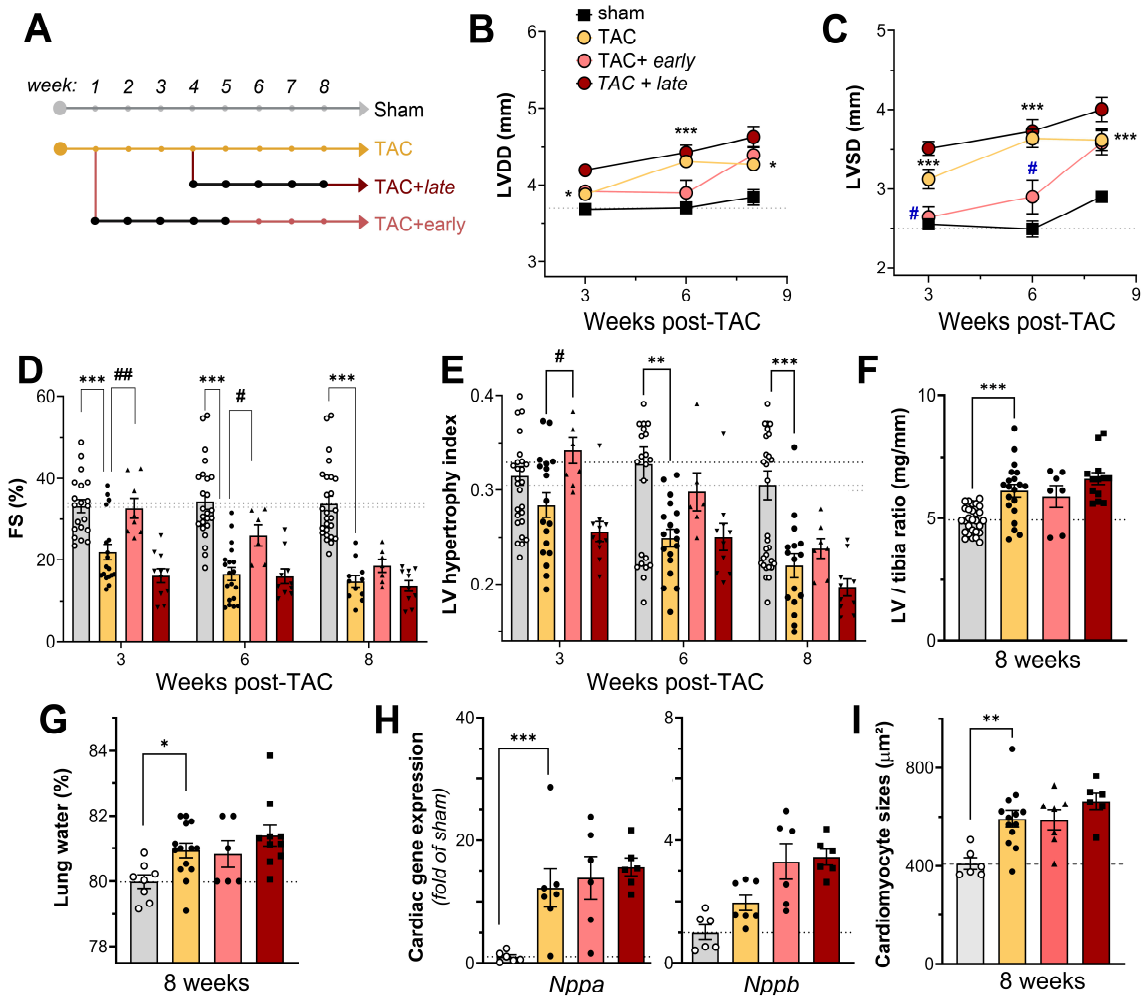

Figure 1 Early anti-IL-1β treatment transiently delays LV dilation but does not impact HF development at 8 weeks post-TAC in BALB/c mice

Schematic overview of the study (**a**). Echocardiography at 3, 6 and 8 weeks post-TAC in sham (*n=29;* grey bars w. white circles), control TAC (*n=18;* yellow bars w. black circles), and *early* (*n=8;* red bars w. black circles) vs. *late* (n=*10;* red bars w. black squares) anti-IL-1β-treated TAC mice was used to assess LV diastolic diameter (*LVDD*, **b**) and LV systolic diameter (*LVSD*, **c**), and to calculate fractional shortening (*FS*, **d**). LV hypertrophy dilatation index (**e**) Morphometric assessment of left ventricular (LV) weights normalized to tibia lengths at 8 weeks (**f**), and lung water content (**g**). Cardiac expression analyses at 8 weeks of *Nppa* and *Nppb* (**h**, *n= 6-7* per group). Analysis and examples of cardiomyocyte cross-sectional area (**i**, *n=6-13* animals per group) at 8 weeks. Mean ± s.e.m are shown. Groups were compared by two-way ANOVA followed by Dunnett's multiple comparison test (panels **b-e, i**), by one-way ANOVA followed by Sidak's multiple comparison test (**g, h**), or by non-parametric Kruskal Wallis followed by Dunn's posthoc test (**i**) * p<0.05, ** p<0.01, *** p<0.001 *versus* sham; # p<0.05; ## p<0.01 *versus* TAC control.

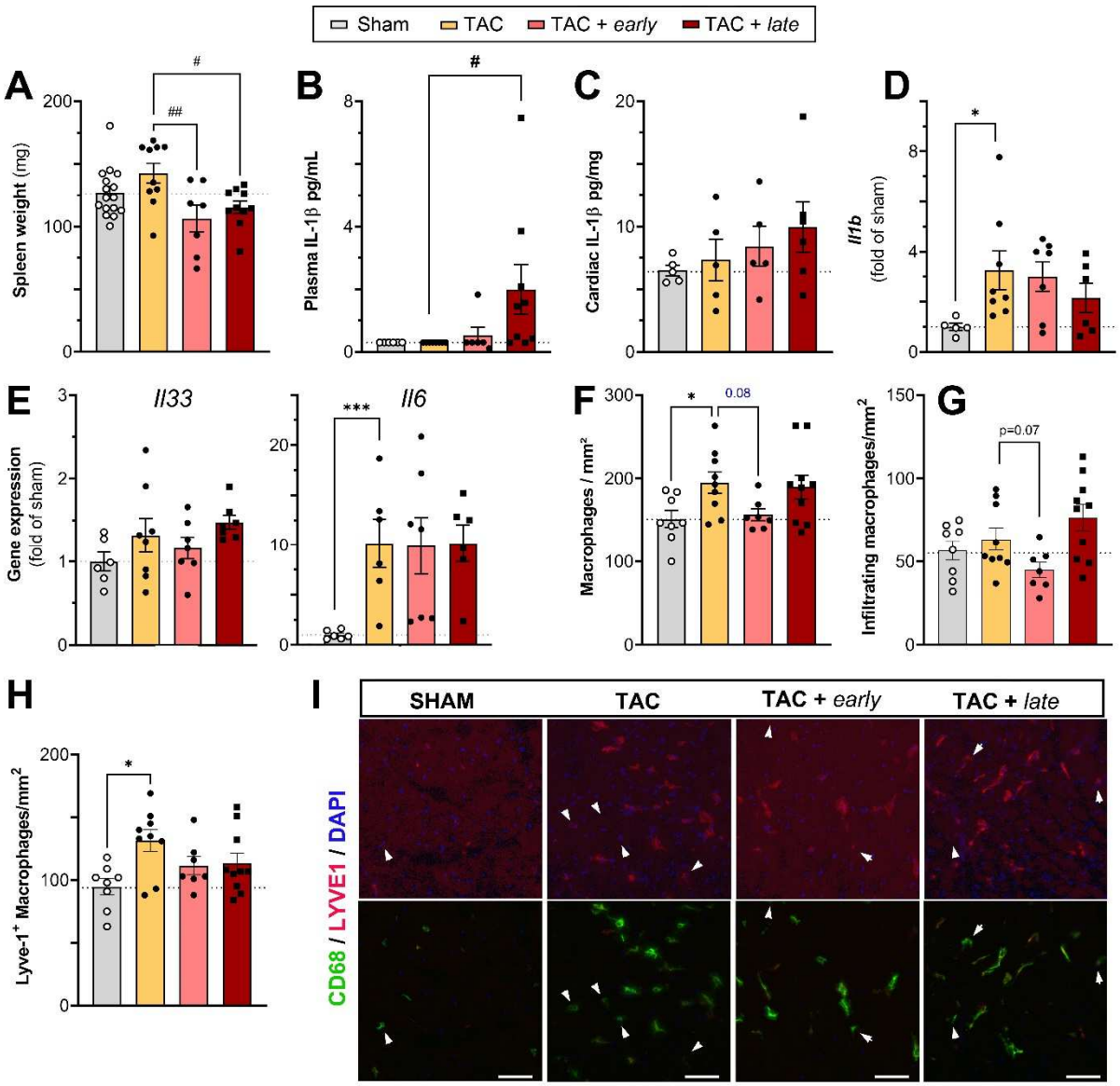

Figure 2 Anti-IL-1β treatment has weak impact on cardiac inflammation post-TAC

Morphometric assessment of spleen weights at 8 weeks (**a**) in sham (*n=16;* grey bars w. white circles), control TAC (*n=10;* yellow bars w. black circles), and *early* (*n=7;* red bars w. black circles) vs. *late* (n=*10;* red bars w. black squares) anti-IL-1β-treated TAC mice. Plasma (**b**) and cardiac (**c**) IL-1β protein levels evaluated by ELISA at 8 weeks post-TAC (*n=5-10* mice per group). Cardiac *Il1b* (**d**), and *Il33* and *Il6* gene expression (**e**) evaluated by qPCR at 8 weeks post-TAC (*n=5-8* mice per group). Quantification of total cardiac CD68⁺ macrophage levels evaluated by immunohistochemistry at 8 weeks (**f**). Quantification of infiltrating CD68⁺Lyve1⁻ macrophages (**g**) and tissue-resident CD68⁺ / Lyve1⁺ macrophages (**h**) (*n=7-10* mice per group). Examples of cardiac macrophages (**i**). CD68, *green*, Lyve1, *red*, Dapi *blue*, Scalebar 50 µm. Arrowheads point to infiltrating CD68⁺/Lyve1⁻ macrophages. Mean ± s.e.m are shown. Groups were compared by one-way ANOVA followed by Sidak's multiple comparison test (**a, c**), by non-parametric Kruskal Wallis followed by Dunn's multiple comparison posthoc test (**b, e, g, h**), or by mixed-effect analysis followed by Sidak's multiple comparison test (**d**). * p<0.05, *** p<0.001 *versus* sham; # p<0.05; ## p<0.01 *versus* TAC control.

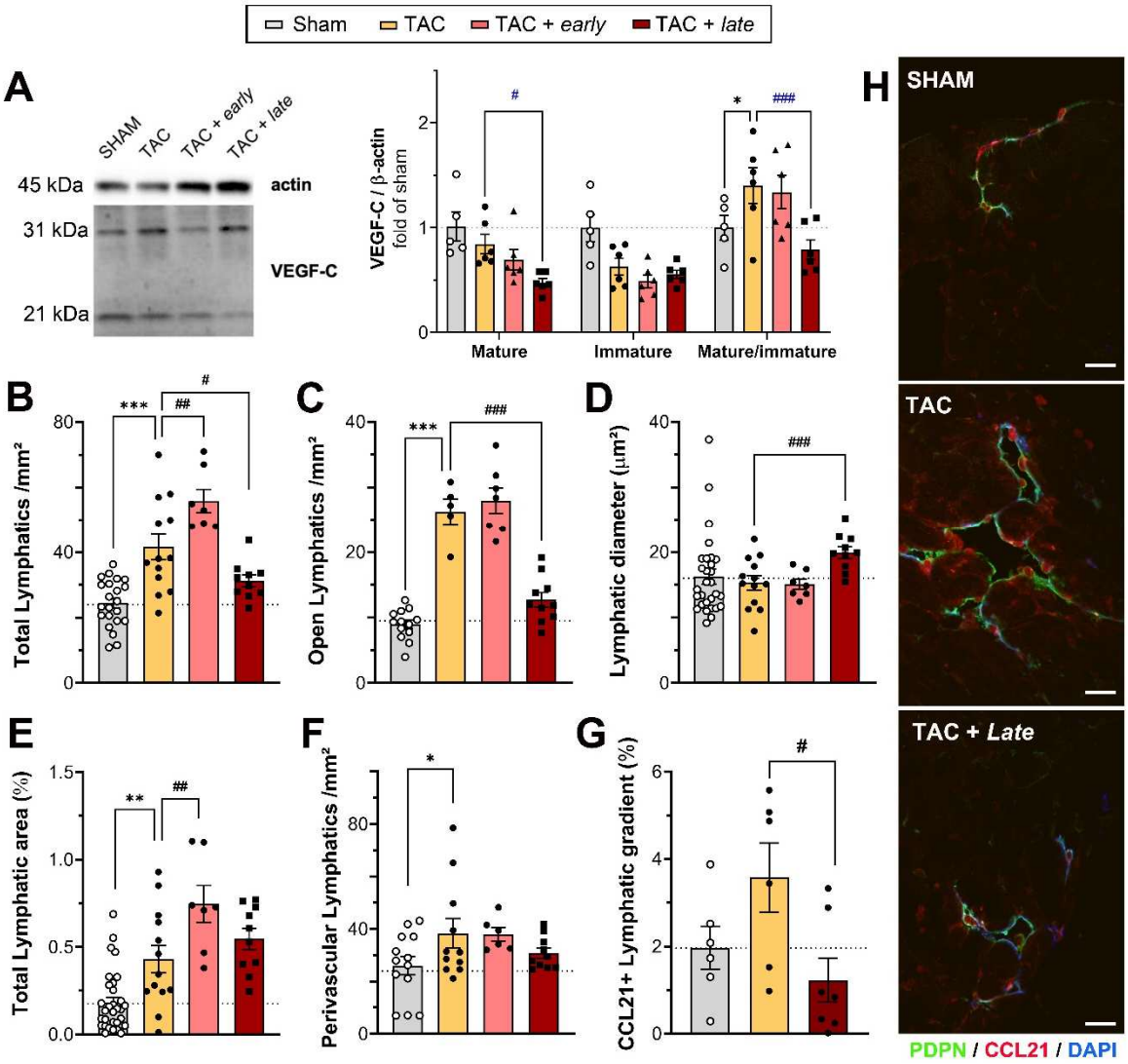

Figure 3 ***Late*** **anti-IL-1β treatment reduces TAC-induced cardiac lymphangiogenesis**

Examples and quantification (**a**) of VEGF-C protein levels (21 kDa mature vs 31 kDa immature monomeric isoforms) in cardiac samples at 8 weeks post-TAC in sham (*n=5;* grey bars w. white circles), control TAC (*n=5;* yellow bars w. black circles), and *early* (*n=5;* red bars w. black circles) vs. *late* (n=*5;* red bars w. black squares) anti-IL-1β-treated TAC mice. Cardiac capillary lymphatic density (**b**), open vessel density (**c**), lymphatic vessel lumen sizes (**d**), lymphatic vascular area (**e**), and perivascular lymphatic density (**f**) were evaluated in histological sections at 8 weeks post-TAC (*n= 6-13* mice per group). Quantification of CCL21 gradients in cardiac lymphatics (**g**). Examples of cardiac lymphatic chemokine gradients (**h**): Podoplanin (PDPN), *green*; CCL21, *red*, Dapi *blue*. Scalebar 50 µm. Mean ± s.e.m are shown. Groups were compared by non-parametric Kruskal Wallis followed by Dunn's posthoc test (**b, c, d, e, f, g**) or by two-way ANOVA followed by Dunnett's multiple comparisons test (**a**). * p<0.05 *versus* sham, ## p<0.01, ### p<0.001 *versus* TAC control.

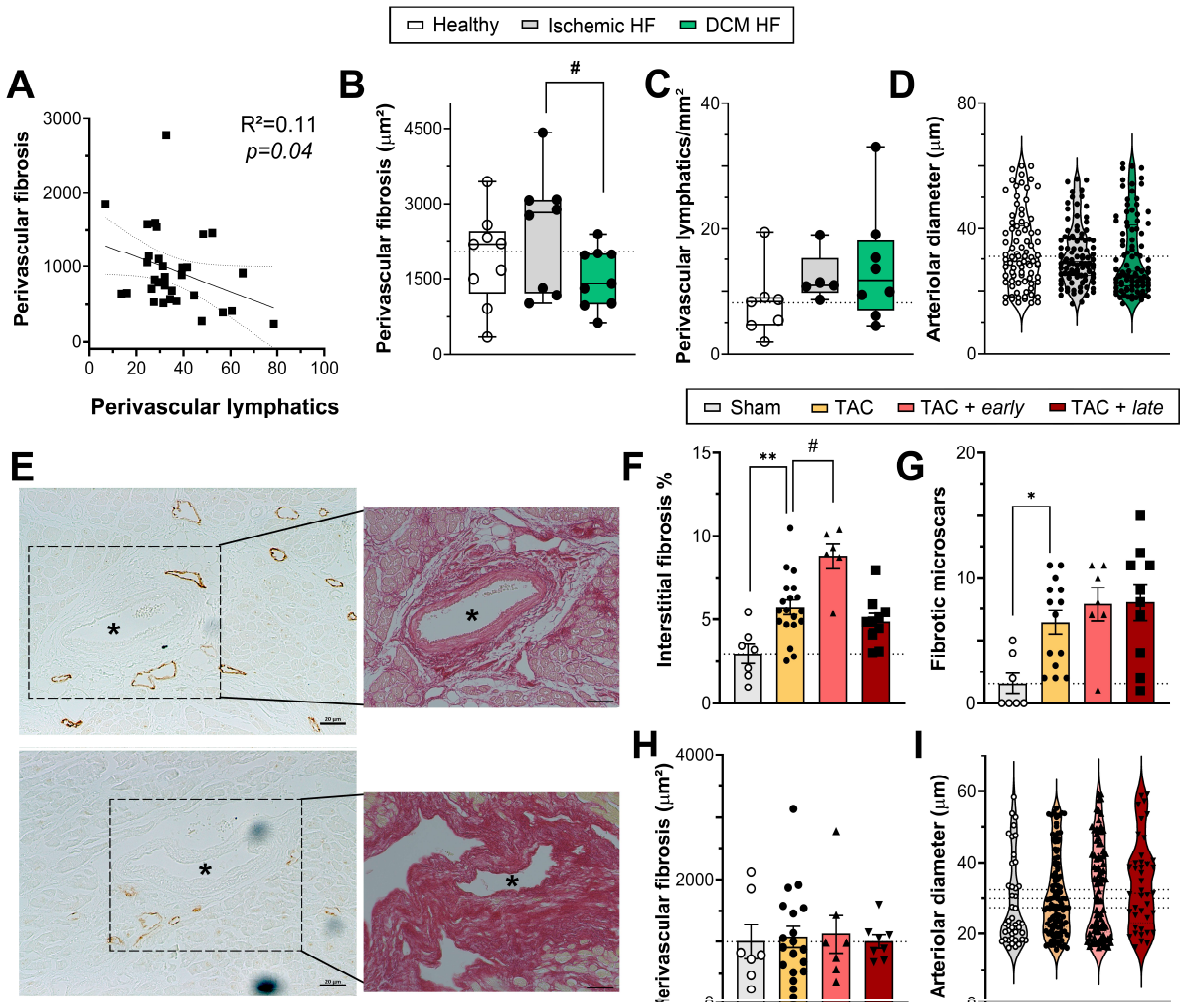

Figure 4 Cardiac perivascular fibrosis post-TAC in mice and HF patients linked to perivascular lymphatics, independently of IL-1β

Correlation analysis of perivascular fibrosis (µm²) and perivascular lymphatic density (vessels/mm²) around coronary arteries in mice at 8 weeks post-TAC (**a**). Quantification of perivascular fibrosis (µm²) in healthy controls (*n=9*, white bar), ischemic HF patients (*n=8, grey bar*), and DCM patients (*n=9, green bar*) (**B**). Arteriolar sizes for evaluation of perivascular fibrosis in patients (**c**). Quantification of perivascular lymphatic densities in patients (**d**, adapted from Heron *et al.*[11]). Examples (**e**) of cardiac perivascular lymphatics, stained for PDPN, and perivascular fibrosis in Sirius Red-stained clinical HF samples; scalebar 20 µm. Evaluation of interstitial fibrosis (**f**) at 8 weeks post-TAC in sham (*n=7;* grey bars w. white circles), control TAC (*n=19;* yellow bars w. black circles), and *early* (*n=6;* red bars w. black circles) vs. *late* (n=*10;* red bars w. black squares) anti-IL-1β-treated TAC mice. Quantification of microscars (**g**) and perivascular fibrosis (**h**) at 8 weeks post-TAC. Arteriolar sizes for evaluation of perivascular fibrosis in mice (**i**). Mean ± s.e.m are shown (**f, g, h**), or violin or box plot with median indicated (**b, c, d, i**). Groups compared by one-way ANOVA followed by Sidak's multiple comparison test (**c, i**) or by non-parametric Kruskal Wallis followed by Dunn's posthoc test (**b, d, f, g, h**). * p<0.05; ** p<0.01 *versus* sham; # p<0.05 *versus* TAC control or DCM patients. Non-parametric Spearman rank order test was used for correlation (**a**).

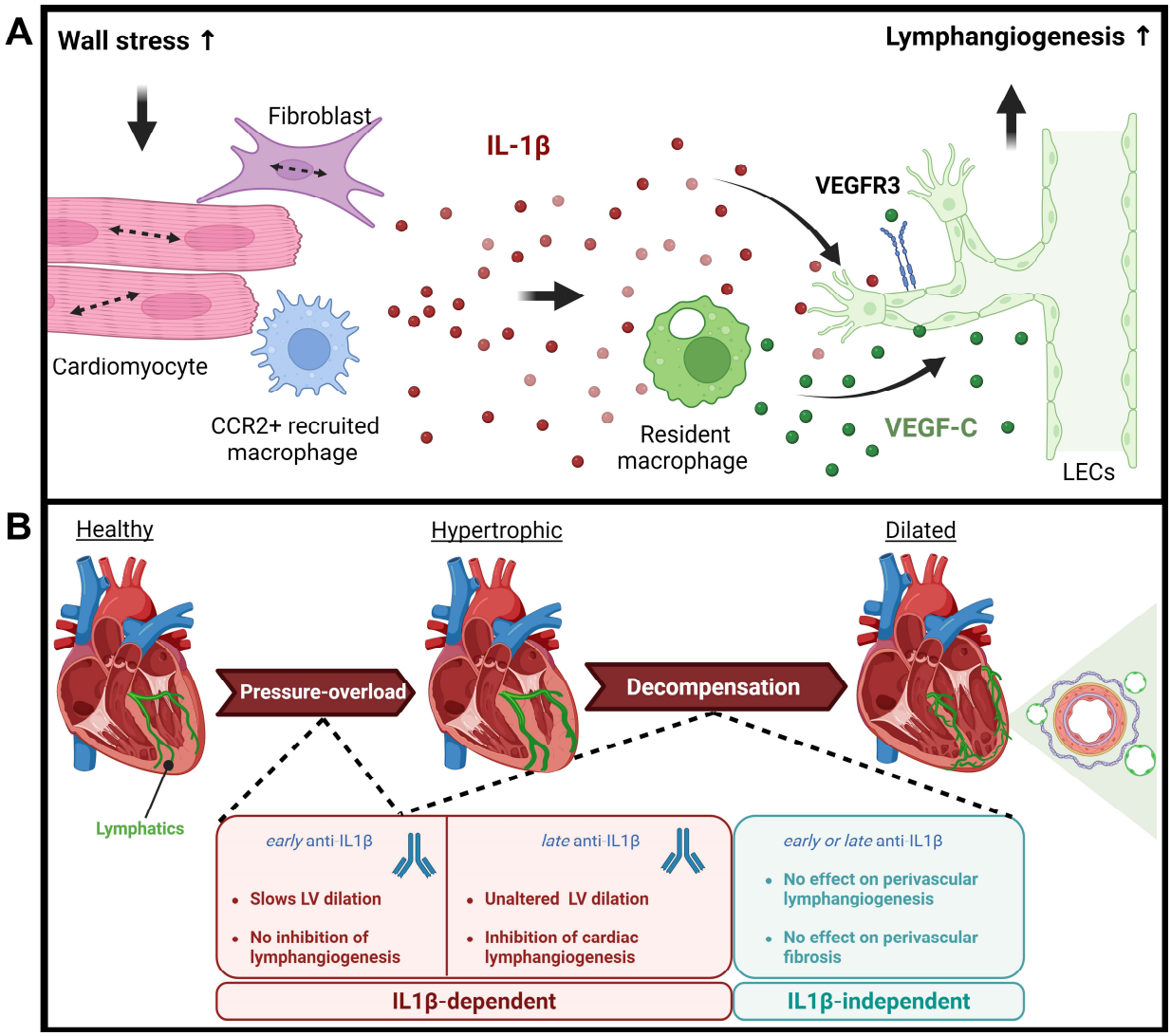

Figure 5 Schematic view of cardiac impact of IL-1β during pressure-overload

In response to increased wall stress (**a**), cardiac cells, including cardiomyocytes, fibroblasts and CCR2⁺ recruited macrophages, release IL-1β. This stimulates both production and maturation of VEGF-C in resident cardiac macrophages. In parallel, IL-1β acts on LECs to increase VEGFR3 (*Flt4*) expression. Together, these changes lead to stimulation of cardiac lymphangiogenesis. In cardiac pathology (**b**), LV dilation triggers IL-1β-dependent macrophage-mediated stimulation of cardiac lymphangiogenesis. However, in the setting of cardiac inflammation, the expanded lymphatic network remains immature and/or dysfunctional, and fails to limit accumulation of immune cells, edema, and interstitial fibrosis. In contrast, perivascular lymphangiogenesis, triggered in an IL-1β-independent manner during LV dilation, limits perivascular fibrosis. Antibody-mediated blockage of IL-1β in *early* phase post-TAC in BALB/c mice, before the onset of lymphangiogenesis, transiently limits LV dilation. In contrast, *late* anti-IL-1β treatment, initiated during LV dilation, blocks cardiac lymphangiogenesis, but not perivascular lymphangiogenesis, and does not alter cardiac remodelling or dysfunction. Created with BioRender.com.

Table 1 – Echocardiography at 8 weeks post-TAC in BALB/c mice

parameter		Sham n=8	p	TAC n=26	TAC + *early* n=7	p	TAC + *late* n=10	p
BW	*g*	**26**±0.4	*ns*	**25**±0.4	**23**±1.2	*ns*	**26**±0.5	*ns*
HR	*bpm*	**338**±8	*ns*	**368**±11	**380**±20	*ns*	**345**±12	*ns*
AWT ED	*mm*	**0.7**±0.05	*ns*	**0.8**±0.02	**0.8**±0.06	*ns*	**0.8**±0.03	*ns*
AWT ES	*mm*	**0.9**±0.04	*	**1.0**±0.03	**1.1**±0.04	*ns*	**0.9**±0.04	*ns*
PWT ED	*mm*	**0.7**±0.03	*ns*	**0.8**±0.03	**0.8**±0.05	*ns*	**0.8**±0.03	*ns*
PWT ES	*mm*	**0.9**±0.03	*ns*	**1.0**±0.04	**1.0**±0.07	*ns*	**0.9**±0.02	*ns*
LVDD	*mm*	**3.8**±0.1	*	**4.3**±0.06	**4.4**±0.1	*ns*	**4.6**±0.1	*ns*
LVSD	*mm*	**2.9**±0.1	***	**3.6**±0.1	**3.6**±0.2	*ns*	**4.0**±0.2	*ns*
FS	*%*	**24**±1.8	*	**17**±1.1	**19**±2	*ns*	**14**±1	*ns*
VTI	*cm*	**2.3**±0.3	*ns*	**1.8**±0.09	**2.4**±0.2	*ns*	**1.7**±0.2	*ns*
SV	*µL*	**58**±6	*ns*	**46**±3	**64**±7	*ns*	**50**±6	*ns*
CO	*mL/min*	**19**±2	*ns*	**17**±1	**24**±3	*ns*	**17**±2	*ns*
EDV	*µL*	**64**±4	*ns*	**72**±5	**55**±6	*ns*	**100**±3	**
ESV	*µL*	**32**±2	***	**62**±4	**88**±5	**	**72**±6	*ns*
EF	*%*	**49**±3	**	**35**±2	**38**±3	*ns*	**29**±3	*ns*

BW, body weight; *HR*, heart rate; *AWT ED*, anterior wall thickness end-diastole; *AWT ES*, anterior wall thickness end-systole; *PWT ED*, posterior wall thickness end-diastole; *PWT ES*, posterior wall thickness end-systole; *LVDD*, left ventricular diastolic diameter; LVSD, left ventricular systolic diameter; *FS*, fractional shortening: *VTI*, velocity time integral; *SV*, stroke volume; *CO*, cardiac output; *EDV*, end diastolic volume; *ESV* end systolic volume; *EF*, ejection fraction. Data reported as mean ± sem. Samples were compared using Two-way ANOVA followed by Sidak's multiple comparison test. * p<0.05; ** p<0,001; *** p<0.001 *versus* TAC controls.

Table 2 – IL-1β-induced gene expression in macrophages in vitro

Gene	*4h*			*24h*		
	Control *n=10-14*	IL-1β *n=10-14*	*p*	Control *n=7*	IL-1β *n=13-14*	*p*
Adamts3	**1.0 ± 0.06**	**1.7 ± 0.17**	***	**1.0 ± 0.06**	**1.9 ± 0.20**	**
Adamts14	**1.0 ± 0.07**	**1.2 ± 0.05**	*n.s*	**1.0 ± 0.10**	**1.1 ± 0.10**	*n.s*
Ctsd	**1.0 ± 0.07**	**1.2 ± 0.14**	*n.s*	**1.0 ± 0.06**	**1.1 ± 0.07**	*n.s*
Ccbe1	**1.0 ± 0.05**	**1.7 ± 0.08**	***	**1.0 ± 0.04**	**1.4 ± 0.12**	*n.s*
Furin	**1.0 ± 0.05**	**1.1 ± 0.06**	*n.s*	**1.0 ± 0.04**	**1.3 ± 0.05**	**
Pcsk5	**1.0 ± 0.08**	**0.6 ± 0.08**	**	**1.0 ± 0.04**	**0.8± 0.15**	*n.s*
Pcsk7	**1.0 ± 0.04**	**1.0 ± 0.04**	*n.s*	**1.0 ± 0.07**	**1.1 ± 0.08**	*n.s*
Vegfc	**1.0 ± 0.05**	**1.7 ± 0.07**	***	**1.0 ± 0.05**	**1.3 ± 0.07**	*

Adamts, A Disintegrin And Metalloproteinase with Thrombospondin Motifs; *Ctsd*, Cathepsin D; *Ccbe1*, collagen- and calcium-binding EGF-like domains 1; *Pcsk,* proprotein convertase. Data reported as mean ± sem. Samples were compared using Two-way ANOVA (mixed-effects model) followed by Sidak's multiple comparison test. * p<0.05; ** p<0,001; *** p<0.001 *versus* untreated controls.

Supplementary methods & materials

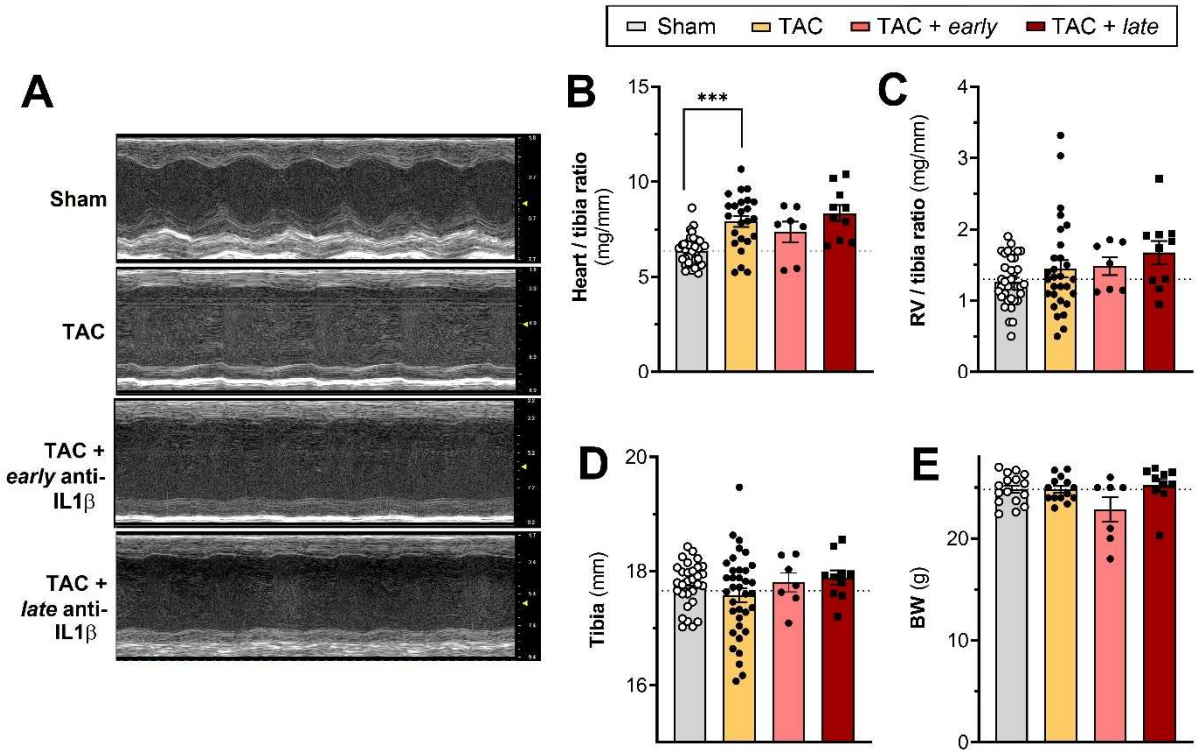

Suppl. Fig. 1- Morphometric analyses at 8 weeks post-TAC

Examples of echocardiography short-axis views (**a**). Assessment of cardiac (**b**) and right ventricular (RV) weights (**c**), normalized to tibia lengths (**d**), and body weight (**e**) at 8 weeks in sham (*n=16-30;* grey bars w. white circles), control TAC (*n=10-36;* yellow bars w. black circles), and *early* (*n=7;* red bars w. black circles) vs. *late* (n=*10;* red bars w. black squares) anti-IL-1β-treated TAC mice. Data reported as mean ± sem. Groups were compared by one-way ANOVA followed by Sidak's multiple comparison test * p<0.05 *versus* sham, ## p<0.01, ### p<0.001 *versus* TAC control.

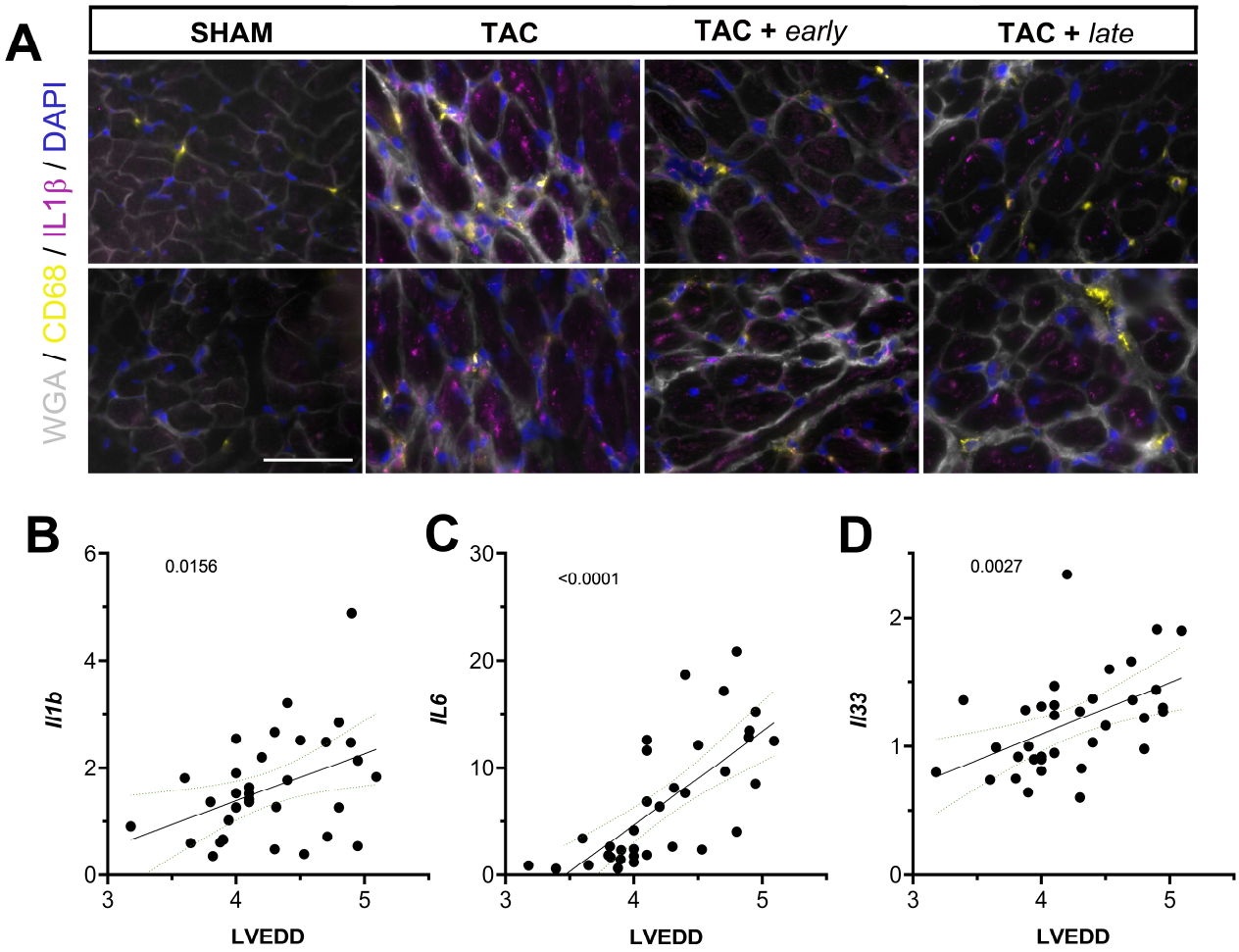

Suppl. Fig. 2 -Correlation between LV EDD and cardiac cytokine expression

Immunohistochemical analyses of IL-1β levels in the heart at 8 weeks in sham, control TAC, and *early* vs. *late* anti-IL-1β-treated TAC mice (**a**). Wga, *grey*; macrophages (CD68), *yellow*; IL-1β, *magenta*; and Dapi, *blue*. Scale bar 50 µm. Evaluation of the degree of LV dilation (LV EDD) and cardiac gene expression levels (*fold of sham*) of *Il1b* (**b**), *Il6* (**c**), and *Il33* (**d**) at 8 weeks post-TAC in BALB/c mice. Non-parametric Spearman rank order tests were used for evaluating correlations.

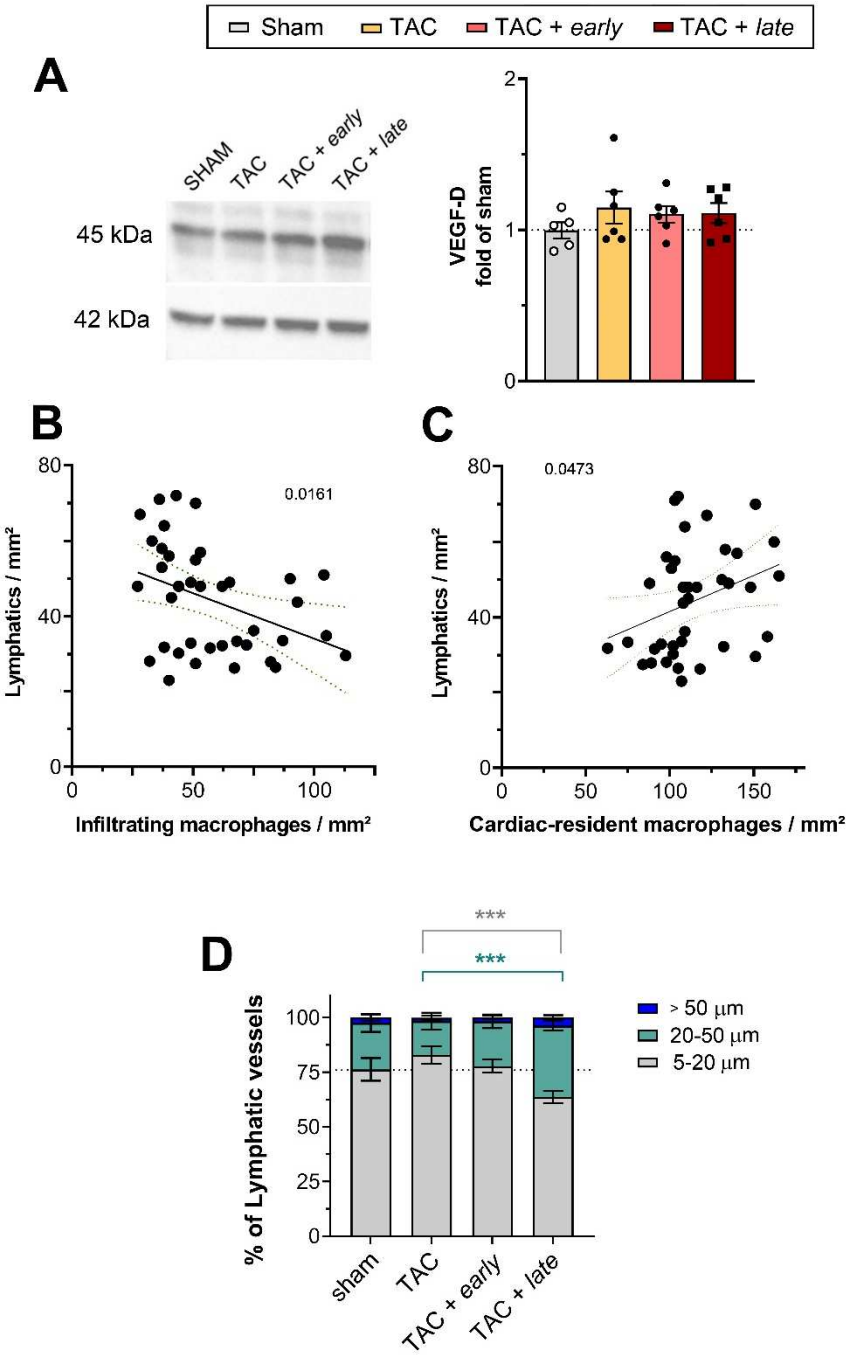

Suppl. Fig. 3 -Cardiac VEGF-D levels and vessel size profiles post-TAC

Western blot examples and quantification of cardiac samples at 8 weeks for VEGF-D (*42 kDa*) protein levels in sham (*n=5;* grey bars w. white circles), control TAC (*n=5;* yellow bars w. black circles), and *early* (*n=5;* red bars w. black circles) vs. *late* (n=*5;* red bars w. black squares) anti-IL-1β-treated TAC mice as compared to actin (*45 kDa*) (**a**). Correlation between cardiac-infiltrating macrophages (**b**) or resident CD68⁺ LYVE1⁺ macrophages (**c**) versus lymphatic densities post-TAC. Evaluation of lymphatic lumen size profiles at 8 weeks post-TAC (**d**) (on average 39 vessels analyzed/mouse: *n=10* mouse/group). Data reported as mean ± sem. Groups were compared by one-way ANOVA followed by Sidak's multiple comparison test, ### p<0.001 *versus* TAC control.

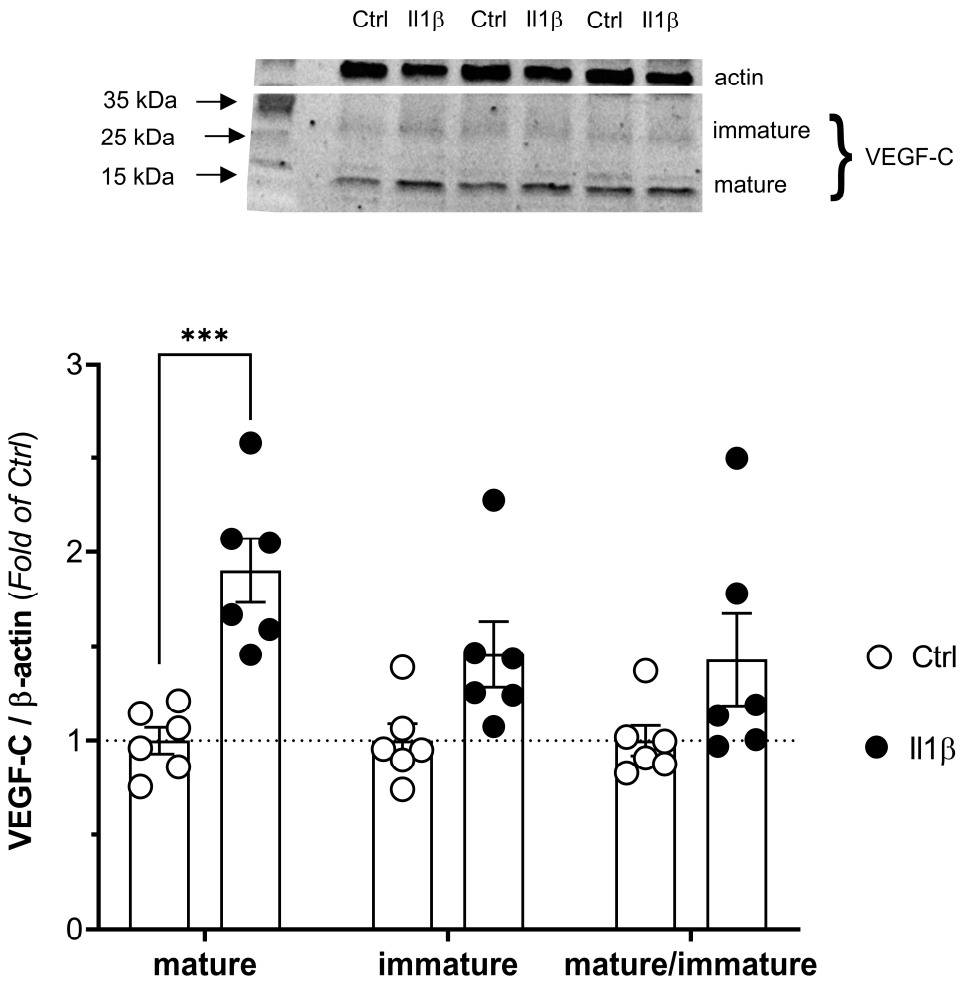

Suppl. Fig 4 – VEGF-C maturation induced by IL-1β in macrophages

Examples and quantification of Western blot analysis of VEGF-C levels in macrophage-conditioned media at 24h of culture in control condition (*open circles, n=6*) or after stimulation with IL-1β (*closed circles, n=6*). Actin band (*45 kDa*), immature VEGF-C (*31 kDa*), and mature VEGF-C (*15-21 kDa*) forms were quantified. Data reported as mean ± sem (fold of control) of averages of 3 separate experiments. Groups were compared by Two-way ANOVA followed by Sidak's multiple comparison test. *** $p<0.001$ *versus* Ctrl.

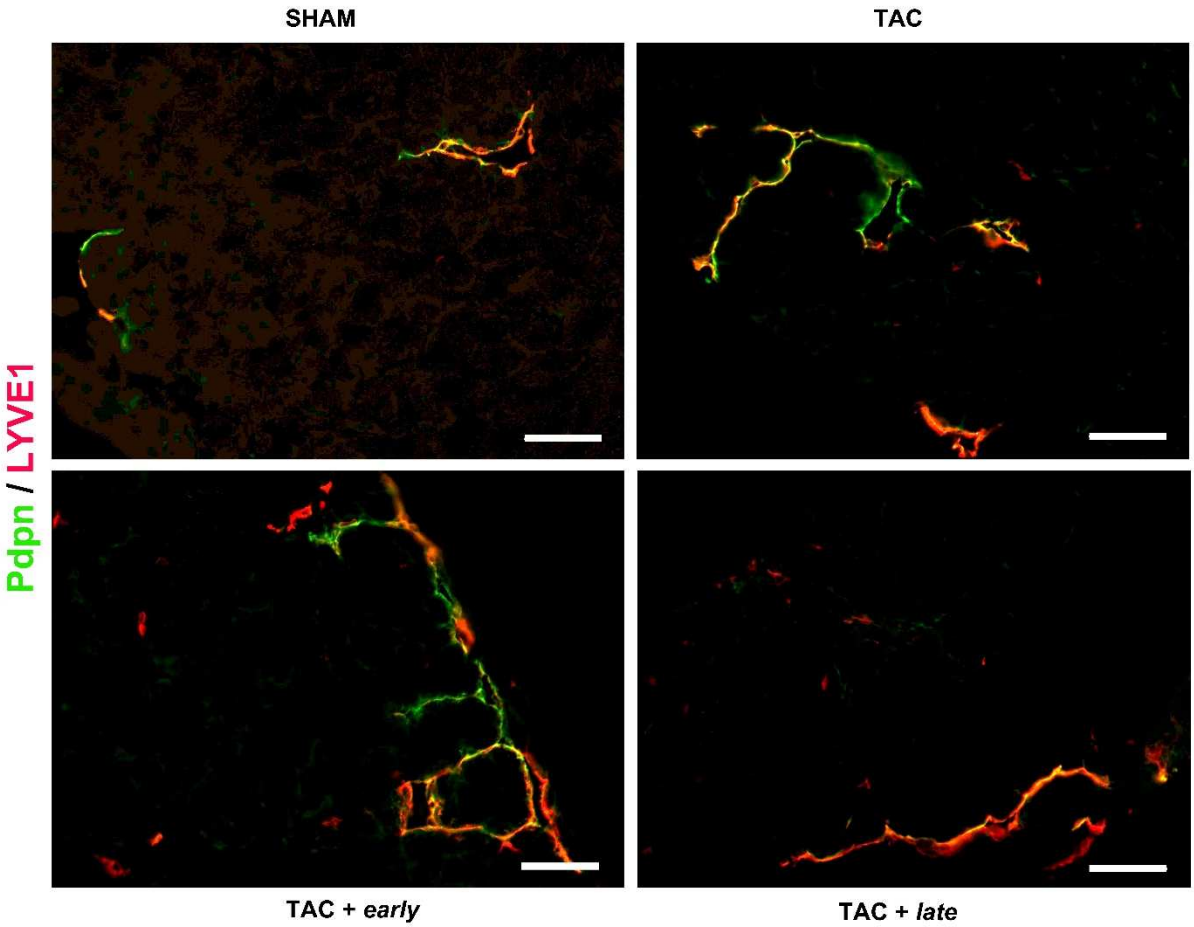

Suppl. Fig. 5 -Cardiac lymphatic network post-TAC

Evaluation of lymphatic vessel densities at 8 weeks post-TAC using a combination of LYVE1 (*red*) and Podoplanin (Pdpn, *green*) in cardiac sections. Scalebar 50 µm.

Suppl. Table 1 – Cardiac function evaluated by echocardiography at 6-weeks post-TAC

parameter		Sham		TAC	TAC + *early*		TAC + *late*	
n		*26*	*p*	*33*	*7*	*p*	*10*	*p*
HR	*bpm*	**355**±9	*n.s*	**382**±9	**443**±31	*n.s*	**391**±14	*n.s*
AWT ED	*mm*	**0.8**±0.03	**	**0.9**±0.02	**0.8**±0.07	*n.s*	**0.9**±0.03	*n.s*
AWT ES	*mm*	**1.2**±0.05	*n.s*	**1.2**±0.04	**1.21**±0.1	*n.s*	**1.2**±0.05	*n.s*
PWT ED	*mm*	**0.8**±0.04	*n.s*	**0.9**±0.03	**0.8**±0.04	*n.s*	**0.8**±0.04	*n.s*
PWT ES	*mm*	**1.1**±0.06	*n.s*	**1.1**±0.03	**1.1**±0.04	*n.s*	**1.0**±0.05	*n.s*
LVDD	*mm*	**3.7**±0.06	***	**4.3**±0.06	**3.9**±0.2	*n.s*	**4.4**±0.1	*n.s*
LVSD	*mm*	**2.5**±0.1	***	**3.6**±0.08	**2.9**±0.2	*	**3.7**±0.1	*n.s*
FS	*%*	**33**±2	***	**18**±1.1	**26**±3	*	**16**±1.8	*n.s*
VTI	*cm*	**1.9**±0.1	*n.s*	**2.0**±0.2	**2.3**±0.1	*n.s*	**1.8**±0.1	*n.s*
SV	*µL*	**56**±3	*n.s*	**60**±7	**59**±5	*n.s*	**47**±5	*n.s*
CO	*mL/min*	**20**±1	*n.s*	**23**±3	**26**±3	*n.s*	**18**±2	*n.s*
EDV	*µL*	**60**±3	***	**77**±4	**35**±6	***	**89**±4	*n.s*
ESV	*µL*	**24**±2	***	**60**±4	**67**±7	*n.s*	**61**±5	*n.s*
EF	*%*	**62**±3	***	**39**±2	**51**±4	*n.s*	**34**±3	*n.s*

BW, body weight; *HR*, heart rate; *AWT ED*, anterior wall thickness end-diastole; *AWT ES*, anterior wall thickness end-systole; *PWT ED*, posterior wall thickness end-diastole; *PWT ES*, posterior wall thickness end-systole; *LVDD*, left ventricular diastolic diameter; LVSD, left ventricular systolic diameter; *FS*, fractional shortening: *VTI*, velocity time integral; *SV*, stroke volume; *CO*, cardiac output; *EDV*, end diastolic volume; *ESV* end systolic volume; *EF*, ejection fraction. All samples were compared using Two-way ANOVA followed by Sidak's posthoc test. * p<0.05; ** p<0,001; *** p<0.001 *versus* TAC controls.

Suppl. Table 2 –LEC gene expression after 24h IL1β stimulation *in vitro*

gene	Ctrl *n=3*	Il-1β *n=3*	*p*
Adamts3	*N.D*	*N.D*	
Adamts14	*N.D*	*N.D*	
Ctsd	1.0 ± 0.0	1.0 ± 0.0	*n.s*
Ccbe1	*N.D*	*N.D*	
Furin	1.0 ± 0.0	**0.9 ± 0.0**	****
Psck5	*N.D*	*N.D*	
Pcsk7	1.0 ± 0.0	1.0 ± 0.0	*n.s*
Flt4	1.0 ± 0.0	**1.5 ± 0.0**	****
Vegfc	*N.D*	*N.D*	
Vegfd	1.0 ± 0.2	1.0 ± 0.1	*n.s*

N.D, not detectable, *Adamts*, A Disintegrin And Metalloproteinase with Thrombospondin Motifs; *Ctsd*, Cathepsin D; *Ccbe1*, collagen- and calcium-binding EGF-like domains 1; *Pcsk,* proprotein convertase; *Flt4*, VEGFR3. Data reported as mean ± sem. **** p<0.0001 *versus Ctrl.*

Suppl. Table 3 – Cardiac gene expression at 8 weeks post-TAC

gene	Sham *n=6*	*p*	TAC *n=8*	TAC + *early* *n=7*	*p*	TAC + *late* *n=7*	*p*
Lyve1	**1.00**±0.05	*n.s*	**1.14**±0.18	**1.41**±0.17	*n.s*	**2.20**±0.17	***
Pdpn	**1.00**±0.11	***	**2.21**±0.28	**2.25**±0.35	*n.s*	**2.12**±0.09	*n.s*
Ccl21	**1.00**±0.09	*n.s*	**1.21**±0.14	**1.44**±0.23	*n.s*	**1.91**±0.13	*
Vegfc	**1.00**±0.06	*	**1.65**±0.13	**1.82**±0.18	*n.s*	**1.71**±0.08	*n.s*
Vegfd	**1.00**±0.09	*n.s*	**1.48**±0.3	**1.12**±0.08	*n.s*	**0.88**±0.08	*

All samples were compared using Two-way ANOVA followed by Sidak's posthoc test.
* p<0.05; ** p<0,001; *** p<0.001 *versus* TAC controls.

Suppl. Methods & Materials

Human samples

Five micrometer thick sections were prepared from paraffin-embedded human septal samples. Standard immunohistological protocols, including citrate antigen retrieval, were used to reveal podoplanin-positive lymphatic vessels using a mouse anti-human podoplanin/D2-40 antibody validated for clinical practice (Dako, # M3619, diluted *1:50*). Signal was revealed following incubation with HRP-conjugated donkey anti-mouse secondary, followed by DAB detection kit (Vector Laboratories, Burlingame, CA). All patient slides were processed together for uniformity. Lymphatics were examined using a Zeiss axiovision light microscope equipped with CCD cameras at *x10.* Lymphatic vessels, identified as Podoplanin$^+$ vascular structures in the subendocardium, were counted by an observer blinded to the patient category. Total lymphatic density, open lymphatic density (lumenized vessels), lymphatic vessel diameter, and density of perivascular lymphatics (defined as lymphatics within 200 µm distance of a large blood vessel) were determined. On average for each patient 1.2 ±0.2 mm² of the septal sample was analyzed to determine lymphatic vessel sizes and densities.

Experimental Model

Female BALB/c mice (22-24 g) were obtained from Janvier. Animal housing and experiments were in accordance with National Institutes of Health guidelines, and the study was ethically approved by the Normandy University regional review board according to French and EU legislation (APAFIS #**23175**-2019112214599474 v6; APAFIS #**32433**-2022070712508369 v2). Minimally-invasive transversal aortic banding constriction (TAC) was performed on 8 week-old mice, as previously described.[1] Mice were anaesthetized by intraperitoneal injection of ketamine (100 mg kg $^{-1}$ Imalgene®) and xylazine (10 mg kg $^{-1}$ Rompun® 2%, Bayer Health Care) and placed on mechanical ventilation. The operator performed a minimal thoracotomy with an incision at the level of the first intercostal space. The aortic arch was visualized under low-power magnification. A snare, made of 7-0 polypropylene suture, was passed under the aorta between the origin of the right innominate and left common carotid arteries. Two suture bands were placed side-by-side to create an elongated stenosis and prevent internalization of the suture, as described.[2] A bent 26-gauge needle was placed next to the aortic arch, and the sutures were snugly tied around the needle and the aorta. After banding, the needle was quickly removed. The skin was closed, and mice recovered on a warming pad until fully awake. The sham procedure was identical except that the aorta was not banded. Buprenorphine (50 µg/kg, Buprecare®, Axcience) was injected subcutaneously 6 hours after surgery and twice per day until 3 days post-operation. Anti-IL-1β treatment consisted of a blocking monoclonal antibody against IL-1β, (Gevokizumab/XOMA-052 provided by Servier France), as previously described.[3] The antibody was administered by repeated intraperitoneal injections of 200 µg/mouse (10 mg/kg^{-1}) three times per week starting from week-1 until week-5 post-TAC (*early* treatment) or starting from week-4 until week-8 post-TAC (*late* treatment).

Echocardiography

Transthoracic echocardiography measurements (Doppler and M-mode) were performed in animals anaesthetized with isoflurane (1-2%), using a Vevo 3100 Imaging System (FUJIFILM). The heart was analysed in the two-dimensional mode in parasternal short-axis views. LV fractional shortening and ejection fraction were calculated using M mode imaging. To evaluate heart rate (HR) and velocity time integral (VTI), a pulsed Doppler of the LV outflow tract was performed, allowing calculation of stroke volume (SV = π × LV outflow radius^2 × VTI) and cardiac output (CO = SV × HR). LV outflow radius was measured for each animal. Aortic flow was measured using pulsed Doppler to verify the efficacy of transversal aortic constriction compared to sham mice. Echocardiographic analyses were performed with VevoLAB software.

Immunohistochemistry

Murine cardiac samples were sectioned into a central slice, which was snap-frozen. Cardiac sections were cut on a cryostat (8 µm thickness) and collected on SuperFrost plus glass slides. After fixation in acetone for 10 min, non-specific binding sites were blocked in 3% BSA in PBS, followed by Biotin-Avidin Blocking kit (Thermo Scientific) when streptavidin (SA)-conjugates were used to detect biotinylated secondary antibodies. Primary antibodies (*see Suppl. Table 3*), diluted in 1% BSA in PBS, were incubated on the sections at r.t. for 1h, followed by repeated washing in PBS and incubation with secondary antibodies (*see Suppl. Table 4*) for 30 minutes to 1h. Double or triple stainings were performed sequentially, and negative controls included omission of primary antibodies. Slides were mounted in Vectashield containing DAPI, and images were acquired using x20 or x40 objectives on a Zeiss epifluorescence microscope (AxioImager J1) equipped with an apotome and Zen 2012 software (Zeiss). Images were analyzed by an operator blinded to the treatment groups using Fiji imaging software (NIH).

Suppl. Table 4 – antibodies used for immunohistochemistry in mice

antigen	article	supplier	species reactivity	host	dilution	Conc (µg/mL)
CD68	*14-0681-82*	eBioscience	*mouse*	**rat**	1/800	**5**
CCL21	*AF457*	RnD Systems	*mouse*	**goat**	1/100	**5**
LYVE-1	*103-PA50*	Reliatech	*mouse*	**rabbit**	1/1000	**0.4**
Podoplanin	*14-5381-82*	eBioscience	*mouse*	**hamster**	1/10 000	**1**
IL-1β	*AF401NA*	RnD Systems	*mouse*	**goat**	1/100	**2**
WGA-FITC	*FP-CE8070*	Interchim			1/100	**1**
antigen	article	supplier		Fluorochrome		Conc (µg/ mL)
Donkey anti-Rabbit	*711-165-152*	Jackson Immunoresearch		**Cy3**		**3**
Streptavidin	*FP-CA5640*	Interchim		**Fluoprobe 647**		**0.7**
Biotinylated Donkey anti-Goat	*705-605-147*	Jackson Immunoresearch				**1.9**
Donkey anti-Rat	*712-586-152*	Jackson Immunoresearch		**Cy3**		**3**
Donkey anti-Goat	*A50-201D3*	Interchim		*DYLIGHT 550*		**1.25**
Goat anti-Hamster	*A-21110*	Thermo Fisher Scientific Invitrogen		**AF488**		**0.8**

Image analysis of cardiac sections

Murine lymphatic vessels were defined as strongly Lyve1-positive structures, lacking macrophage markers (CD68), and mostly also positive for Podoplanin. Lymphatics are preferentially located in the subepicardium in rodent hearts. These Lyve1-positive, CD68-negative vessels clearly differ from CD68$^+$ macrophages, which either lack or display weaker

Lyve1 expression. These macrophages, also differing in size and morphology from the elongated cell body and nucleus typical of lymphatic endothelial cells, were readily excluded from lymphatic counts. Photos were captured at *x20*.

Due to the absence of conclusive markers to distinguish precollectors from capillaries in murine cardiac lymphatics, we have made use of the fact that precollectors preferentially run in a base-to-apex fashion, whereas lymphatic capillaries lack such consistent spatial organization. Hence, by evaluating vessels with a lumen parallel to horizontal cardiac sections, the precollector population of vessels is more frequently detected as vessels running perpendicular to the section (= open lumen vessels). To assess the size and frequency of open lymphatic vessels (diameter > 5 µm; a population enriched in precollector vessels), between 10-20 images from the LV free-wall were collected and analyzed for each mouse. The density (open vessels/mm²) and lymphatic lumen sizes were measured and used to calculate mean vessel diameter. The parameter % open lymphatic area was calculated as the sum total of all measured lymphatic diameters divided by the total cardiac area analyzed for each mouse heart. On average for each mouse 2.2±0.3 mm² of the LV was analyzed to determine lymphatic vessel sizes and % open lymphatic area.

Cardiomyocyte sizes were evaluated in sections double stained for CD31 and WGA imaged at *x40*. Cardiac macrophages were defined as CD68 positive cells. Infiltrating macrophages were defined as $LYVE1^-$ cells, and cardiac-resident macrophages as $LYVE1^+$ cells. Images were captured at *x20*.

Histology in mouse or human cardiac sections

Cardiac cryosections (8 µm) of mouse samples, or paraffin sections (5 µm) of human samples, were processed for Sirius Red staining, as described.[1] Cardiac interstitial collagen density was evaluated in mouse cardiac sections imaged on a light microscope (Zeiss) equipped with an *x40* objective. Replacement fibrosis (micro-scars) was evaluated in these images as total number/cardiac section of fibrotic hotspots, identified as images containing >11% fibrotic area per image, analyzing on average 14±0.5 images/sample (average total examined area 0.5 mm² of each LV cross-section). Perivascular fibrosis was evaluated in images taken at *x20,* focused on arterioles with a lumen diameter of 16-60 µm in both mice and men. On average 5 vessels/cardiac section were used to determine perivascular fibrotic area (µm²), as previously described.[4] Images were analyzed by an operator blinded to treatment groups using Fiji imaging software (NIH).

Real-Time Polymerase Chain Reaction

Murine cardiac samples were collected at 8-weeks post-TAC. RNA extraction was performed with Trizol method. Briefly, samples were homogenized (45 sec.) in TRIZOL using Precellys tubes with beads. RNA was obtained after incubation, successively, in chloroform and isopropanol and three washes in ethanol. RNA quality was analyzed by Nanodrop 2000 (Thermo Fisher Scientific). cDNAs were generated using a reverse transcriptase after DNAse treatment. Real-time PCR was performed on a LightCycler 480 (Roche Molecular Biochemicals) with a commercially available mix (FastStart DNA Master SYBR Green I kit; Roche) on white 96-well plates. The reactions were performed in duplicate for each sample. Concentrations were calculated using a standard curve, obtained by serial dilutions of samples from an organ with high expression of the gene of interest. To normalize gene expression, values are expressed as ratios of a reference gene (E2F). Healthy sham animal ratios are then set as 100%, and values in TAC-operated animals are expressed relative to their respective sham controls. The sequences of the specific primers are detailed in *Suppl. Table 5.*

Suppl. Table 5 – list of primers used in mouse cardiac samples for qPCR

gene	sense	antisense	amplicon (bp)
Eef2	GCGAGGACAAAGACAAGGAG	GGGATGGTAAGTGGATGGTG	108
Ccl21	TCCCTACAGTATTGTCCGAGGC	ATCAGGTTCTGCACCCAGCCTT	141
Il1β	TGGACCTTCCAGGATGAGGACA	GTTCATCTCGGAGCCTGTAGTG	148
Il6	TACCACTTCACAAGTCGGAGGC	CTGCAAGTGCATCATCGTTGTTC	116
Il33	CTACTGCATGAGACTCCGTTCTG	AGAATCCCGTGGATAGGCAGAG	136
Lyve1	ACCAGGTAGAGTCAGCGCAGAA	CAGGACACCTTTGCCATTCTTCC	128
Nppa	TACAGTGCGGTGTCCAACACAG	TGCTTCCTCAGTCTGCTCACTC	126
Nppb	TCCTAGCCAGTCTCCAGAGCAA	GGTCCTTCAAGAGCTGTCTCTG	98
Pdpn	ACAACCACAGGTGCTACTGGAG	GTTGCTGAGGTGGACAGTTCCT	116
Vegfc	AGCCCACCCTCAATACCAG	GCTGCTCCAAACTCCTTCC	154
Vegfd	CTCCACCAGATTTGCGGCAACT	ACTGGCGACTTCTACGCATGTC	112

Western blot analysis in cardiac samples

Cardiac protein was extracted using Cell lysis buffer (#895347, RnD Systems) in microbead tissue dissociation tubes (Precellys #P000933-LYSK0-A – 0.5 mL). Twenty-five micrograms of denatured cardiac protein from healthy sham-operated or TAC-operated mice at 8 weeks post-TAC treated or not with anti-IL-1β antibodies, were separated on stain-free 4-20% agarose gels (Criterion TGX Precast Gel, Biorad), followed by blotting with a rabbit anti-VEGFC antibody (#ab9546, Abcam; *1:1000*), or a rabbit anti-VEGFD antibody (#ab155288, RnD systems; *1:500*), and finally a mouse anti-actin antibody (#15597191, Invitrogen; *1:10000*) diluted in PBS/BSA 5%. After repeated washing, HRP-conjugated secondary antibodies (goat anti-rabbit #P0448, Dako; *1:5000*, donkey anti-mouse #A16011, Invitrogen; *1:5000*) were used. Target proteins were visualized using ECL chemiluminescence kit (#1705061, BioRad). Ratios of specific bands to actin signal per well was analyzed in ImageJ. For VEGF-C and VEGF-D multiple bands were present, representing the various cleaved forms of the growth factors. For VEGF-C, the ratio of mature to immature forms was calculated as the ratio of the densities of cleaved, mature monomeric VEGF-C (21 kDa bands) to the densities of full-length immature monomeric pro-VEGF-C (31 kDa bands)[5]. For VEGF-D only the full-length immature pro-VEGF-D form (42 kDa dimer) was visible (cleaved, mature form at 32 kDa too weak for analysis). VEGF-C and VEGF-D protein ratios were compared between sham and TAC groups using two-way ANOVA followed by Sidak's posthoc test.

Samples of macrophage-conditioned media (average protein concentration 1 mg/mL) were prepared with β-mercapto, and 23 micrograms of denatured protein from control or IL-1β-treated cells (n=6 samples/group) were separated on 4-15% precast polyacrylamide gels (Mini-PROTEAN TGX Gels, BioRad), followed by blotting with a rabbit anti-VEGFC antibody (#ab9546, Abcam; 1:200) diluted in TBS-T/BSA 5%. After repeated washing, biotin-conjugated secondary antibodies (biotinylated goat anti-rabbit; 111-065-144, Jackson ImmunoResearch, 1:5000) was used, followed by SA-HRP (N100, Thermoscientific, 1:5000). Subsequently, blots were incubated with a mouse anti-actin antibody (MA5-15739, Invitrogen; 1:5000), followed by a secondary antibody (HRP-conjugated donkey anti-mouse #A16011, Invitrogen; 1:10000). Target proteins were visualized using ECL chemiluminescence kit (#170-5061, BioRad). Ratios of specific bands to actin signal per well were analysed in ImageLab. For VEGF-C, multiple bands were present: a full-length (immature) 31 kDa band and 15-21 kDa cleaved (mature) monomeric band. Levels of each protein form, and the relative ratio of mature to immature VEGF-C, were calculated and presented as fold of control. Data were compared between control and Il-1β treated groups using two-way ANOVA followed by Sidak's posthoc test.

Cell culture

Bone marrow-derived macrophages (BMM) were prepared from femur and tibia of C57/BL6 mice. Briefly, bone marrow-derived cells were seeded in 6-well plates (6×10^6/well) and differentiated into macrophages in RPMI1640 medium containing 15% L929-conditioned medium, 10% fetal calf serum (*FCS*, heat inactivated at 56 °C/ 45min), 50 µM β-mercaptoethanol, 100 U/mL penicillin, and 100 µg/mL streptomycin during 7 days, as described[6]. On day 7, BMMs were serum-starved in RPMI medium containing 0.5% FCS for 4h and exposed for 4 and 24 hours to 10 ng/mL recombinant murine IL-1β (PreproTech, 211-11B) in 0.6 mL per well of 0.5% FCS cell culture media. Total RNA was isolated using NucleoSpin RNA kit (Macherey Nagel, 740955) according the instruction. RNA was transcribed using First Strand cDNA Synthesis Kit (Thermo Scientific, K1612). qPCR was done on GeneQuant Studio 6 Real-Time PCR System using SybrGreen PCR Mix. Primers used in qPCR are listed in *Suppl Table 6*.

Balb/c dermal LECs (CellBiologics, BALB-5064L) were seeded in 6-well plates (3×10^5/well) and grown to confluence in complete Endothelial Cell Medium (ECM, CellBiologics, M1168) including 5% FCS with VEGF, ECGF, EGF supplement, according to recommendations of the supplier. Next, cells were serum-starved (1% FCS, ECM w/o VEGF, ECGF, EGF) overnight, and exposed to 20 ng/mL recombinant mouse IL-1β (PreproTech) in 2 mL per well of serum-starvation media. After 24h cells were recovered and RNA extracted (RNeasy minikit, 74104, Qiagen) for subsequent mRNAseq analyses and bioinformatics analyses by NOVOGENE company (Cambridge, UK) for identification of differentially expressed genes. Briefly, poly-A mRNA-seq, sequencing length of 150 nt paired-end (PE150), were performed with Illumina Seq. Reads were aligned to the mouse genome. Transcript quantification was performed with featureCounts, and differential analysis, including normalization, was performed with DESeq2 bioconductor package. Genes significantly up- or downregulated upon treatment were identified (p-values were adjusted for multiple testing by the Benjamini–Hochberg False Discovery Rate (FDR) procedure). Results are reported as fold of control condition (1% FCS, ECM without cytokines) quantified as FPKM. For full RNAseq data please see *Suppl Table 7*.

Suppl. Table 6 – list of primers used in mouse macrophages for qPCR

gene	sense	antisense	amplicon (bp)
Adamts3	TTCCAGGAACCTCTGTTGCC	GCTGATCTCTTGTAGACAAC	151
Adamts14	CTGATCATGGTGGGCTACCGACA	CCATCCTCGTGGTTGAGGGCACA	236
Ctsd/CatD	AGGTGAAG GAGCTGCAGAAG	ATTCCCATGAAGCCACTCAG	199
Ccbe1	ATGGGACCTATGGGACCTTC	AGTGAGTCCGGTGTCCAAAC	235
Furin	TGAGCCATTCGTATGGCTACG	GGACACAGCTTTTCTGGTGCA	576
Pcsk5	AGGTGGAGTGGATCCAACAG	CCGTGTAGCCTCTCTTCCAG	189
Pcsk7	CCACCCTGATGAGGAGAATG	GCCACAGCCTCCATACTGTC	165
Vegfc	CGAGGTCAAGGCTTTTGAAG	TCCCCTGTCCTGGTATTGAG	165

Adamts, A Disintegrin And Metalloproteinase with Thrombospondin Motifs; *Ctsd*, Cathepsin D; *Ccbe1*, collagen- and calcium-binding EGF-like domains 1; *Pcsk*, proprotein convertase

Suppl. References

1. Heron C, Dumesnil A, Houssari M, Renet S, Lemarcis T, Lebon A, Godefroy D, Schapman D, Henri O, Riou G, Nicol L, Henry JP, Valet M, Pieronne-Deperrois M, Ouvrard-Pascaud A, Hägerling R, Chiavelli H, Michel JB, Mulder P, Fraineau S, Richard V, Tardif V, Brakenhielm E. Regulation and impact of cardiac lymphangiogenesis in pressure-overload-induced heart failure. *Cardiovasc Res* 2023;**119**:492–505.
2. Lygate CA, Schneider JE, Hulbert K, Hove M ten, Sebag-Montefiore LM, Cassidy PJ, Clarke K, Neubauer S. Serial high resolution 3D-MRI after aortic banding in mice: band internalization is a source of variability in the hypertrophic response. *Basic Res Cardiol* 2006;**101**:8–16.

3. Harouki N, Nicol L, Remy-Jouet I, Henry J-P, Dumesnil A, Lejeune A, Renet S, Golding F, Djerada Z, Wecker D, Bolduc V, Bouly M, Roussel J, Richard V, Mulder P. The IL-1β Antibody Gevokizumab Limits Cardiac Remodeling and Coronary Dysfunction in Rats With Heart Failure. *JACC Basic Transl Sci* 2017;**2**:418–430.
4. Dai Z, Aoki T, Fukumoto Y, Shimokawa H. Coronary perivascular fibrosis is associated with impairment of coronary blood flow in patients with non-ischemic heart failure. *J Cardiol* 2012;**60**:416–421.
5. Joukov V, Sorsa T, Kumar V, Jeltsch M, Claesson-Welsh L, Cao Y, Saksela O, Kalkkinen N, Alitalo K. Proteolytic processing regulates receptor specificity and activity of VEGF-C. *EMBO J* 1997;**16**:3898–3911.
6. Rizzo G, Gropper J, Piollet M, Vafadarnejad E, Rizakou A, Bandi SR, Arampatzi P, Krammer T, DiFabion N, Dietrich O, Arias-Loza A-P, Prinz M, Mack M, Schlepckow K, Haass C, Silvestre J-S, Zernecke A, Saliba A-E, Cochain C. Dynamics of monocyte-derived macrophage diversity in experimental myocardial infarction. *Cardiovasc Res* 2023;**119**:772–785.